

Long-term experimental testing of phase change materials as cooling devices for photovoltaic modules

Ortiz Lizcano, Juan Camilo; Ziar, Hesan; de Mooij, Cas; Verheijen, Mario P.F.; van Nierop Sanchez, Chris; Ferlito, Davide; Connelly, Carmelo; Canino, Andrea; Zeman, Miro; Isabella, Olindo

DOI

[10.1016/j.solmat.2024.113133](https://doi.org/10.1016/j.solmat.2024.113133)

Publication date

2024

Document Version

Final published version

Published in

Solar Energy Materials and Solar Cells

Citation (APA)

Ortiz Lizcano, J. C., Ziar, H., de Mooij, C., Verheijen, M. P. F., van Nierop Sanchez, C., Ferlito, D., Connelly, C., Canino, A., Zeman, M., & Isabella, O. (2024). Long-term experimental testing of phase change materials as cooling devices for photovoltaic modules. *Solar Energy Materials and Solar Cells*, 277, Article 113133. <https://doi.org/10.1016/j.solmat.2024.113133>

Important note

To cite this publication, please use the final published version (if applicable).
Please check the document version above.

Copyright

Other than for strictly personal use, it is not permitted to download, forward or distribute the text or part of it, without the consent of the author(s) and/or copyright holder(s), unless the work is under an open content license such as Creative Commons.

Takedown policy

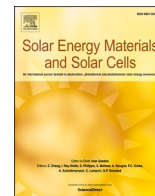
Please contact us and provide details if you believe this document breaches copyrights.
We will remove access to the work immediately and investigate your claim.

Green Open Access added to TU Delft Institutional Repository

'You share, we take care!' - Taverne project

<https://www.openaccess.nl/en/you-share-we-take-care>

Otherwise as indicated in the copyright section: the publisher is the copyright holder of this work and the author uses the Dutch legislation to make this work public.



Long-term experimental testing of phase change materials as cooling devices for photovoltaic modules

Juan Camilo Ortiz Lizcano^{a,*}, Hesam Ziar^{a,**}, Cas de Mooij^a, Mario P.F. Verheijen^a, Chris van Nierop Sanchez^a, Davide Ferlito^b, Carmelo Connelli^b, Andrea Canino^b, Miro Zeman^a, Olindo Isabella^a

^a Photovoltaic Materials and Devices, Delft University of Technology, Mekelweg 4, 2628 CD, Delft, Netherlands

^b ENEL Green Power SpA, Viale Regina Margherita, 125, 00198, Rome, Italy

ABSTRACT

This work is a long-term, interannual, and experimental study conducted in multiple locations. It studies the effects of phase change materials (PCMs) on photovoltaic modules' performance by reducing their operational temperature. Two PV modules were manufactured so that PCM slabs could be mechanically attached to their backside, ensuring contact with the related photovoltaic active area. Experiments were conducted in Delft, Netherlands, from 2019 until 2021 and in Catania, Italy, during the winter and start of spring of 2023. The experiment also considered two installation layouts: building integrated (Delft) and standard rack-mounted (Catania). The measurements showed that the PCM provides significant cooling under both locations, with a temperature reduction of up to 15 °C. In Delft, thermal control could be obtained for most of the sunny hours of the day, even during the summer months. In Catania, the module with PCM presented, on occasion, higher temperatures than its standard counterpart, primarily due to winter-time environmental conditions. However, the PCM provided sufficient thermal control on all conditions, ensuring increased energy yield. This increase ranged from 2.1 to 2.5 % in Delft and 1.3–1.6 % in Italy.

1. Introduction

Thermal management is essential to photovoltaic (PV) system operation and maintenance. Heat generation in PV devices represents a significant loss in electrical efficiency. Moreover, high operational temperatures can also contribute to a significant reduction in the lifetime of PV modules [1]. A module's operating temperature depends on multiple factors besides the environmental conditions under which they operate. The installation layout, for example, can reduce a PV module's capacity for cooling, particularly by hindering convection mechanisms. This is the case of a PV module integrated into the building environment, where the reduced convection leads to significant temperature increases compared to the same module operating under a rack-mounted layout [2].

Technological developments aimed at reducing the operating temperature of PV modules are frequently classified into passive and active technologies. Active cooling techniques focus on improving the convection mechanism by utilizing auxiliary systems to create significant liquid flow rates (that can be either water or other coolants) [3,4]. These systems provide a stable cooling potential but with the added complexity of pumping systems, pipelines, and additional energy needs

[4] and the need of regular maintenance activities. Passive cooling techniques focus on improving the thermal behavior of a PV module via different physical principles. Improving radiative cooling [5], using spectral shields to repel unwanted irradiation [6], and managing thermalization losses via optical filters are some techniques whose working principle has its basis in spectral management of irradiation [7,8]. The spectral management approach aims at tailoring the way a PV module interacts with the incoming irradiation and has the advantage of being independent of the installation layout. However, the technique requires careful and usually complex design, and its benefits are often location dependent. Utilization of fin elements on the backside of PV modules represents another passive cooling technique that aims at improving convection [9–11]. The main drawback of this approach is its dependence on environmental factors, such as windspeeds, and is limited only to specific installation layouts.

Recently, there have been promising results regarding using phase change materials (PCMs) for PV thermal management. PCMs have the potential to provide temperature reductions of tenths of degrees for extended periods of time [12], making them amongst the most promising techniques for improving electrical performance of PV systems. PCMs are usually classified into four main categories: Organic,

* Corresponding author.

** Corresponding author.

E-mail addresses: j.c.ortizlizcano@tudelft.nl (J.C. Ortiz Lizcano), H.Ziar@tudelft.nl (H. Ziar).

Inorganic, Eutectic and Composite PCM [13]. A sizeable amount of research has focused its attention on solid-to-liquid PCMs because of their technical advantages, particularly volume stability, as reviewed by Zhang et al. [14]. PCM materials can be manufactured with a wide range of latent heat (in kJ/l) and melting temperatures values, from salt solutions with melting temperatures below 0 °C and latent heat values ranging from 50 to 200 kJ/l to Fluorides, exhibiting melting temperatures up to 800 °C and very high values of latent heat (in the range of 900–1000 kJ/l). Such a wide span of values means that PCMs are extremely versatile and can be deployed in many applications.

Recent research focused on incorporating, or attaching, PCMs into PV modules has provided valuable information on their cooling potential. Upon reaching its melting temperature, heat produced by the PV module goes into the PCM and it is used for the phase change (e.g. solid to liquid), a process that occurs at constant temperature. The PCM acts as a heat sink and thermally manages the PV module, thus reducing its operational temperature by delaying its increase rate. For PV applications, key physical properties are the chemical stability of the material, high thermal conductivity, high latent heat, and low supercooling effect, in which the PCM maintains a liquid state even at temperatures lower than its solidification threshold [15]. From a safety and reliability perspective, low leakage, low flammability and volume stability are among the most important aspects of selecting a PCM for PV applications.

Properly selected, a PCM can provide substantial cooling potential, as evidenced by a sizeable amount of experimental work. Some examples of research using PCM to reduce the operating temperature of modules include the work of Japs et al. [16] that mechanically attached bags filled with different PCMs on the backside of 30 W PV panels and measured their temperature for one month in the summer of 2013 in Germany, finding differences of 10 °C and 7 °C depending on the PCM utilized. Maiti et al. [17] used metallic enclosures filled with paraffin wax, measuring reductions of between 17 °C and 20 °C. Sharma et al. [18] used the Rubitherm (RT) 42 (melting temperature of 42 °C) alongside metallic fins on the backside of a PV module with different installation layouts, including building integrated concentrated applications (BICPV). Indoor measurements showed a temperature reduction of up to 10.7 °C. A full year experiment carried out in the United Arab Emirates by Hasan et al. [19] implemented PCMs based on RT 42 on a 40 W PV module, finding maximum temperature reductions of 13 °C and increased power output of around 5.9 % compared to a standard module. Stropnik and Strith [20] tested using RT 28 during seven days of October in Ljubljana using a 250 W PV module. The authors observed a PV surface temperature reduction of 35 °C and an average increase in electrical efficiency of 2.8 %. Elavarasan et al. [21] developed a cooling system based on PCM (HS29), fins and a water reservoir (3.3 L) and applied it to a PV module (5 W). The measurements took place during two days of October in Madurai, India. They measured temperature reductions of up to 16.7 °C, and a relative increase in power output of 9 %. Kumar et al. [22] used a phase change material fabricated from a mixture of copper, silicon carbide and paraffin wax. The authors measured temperature reductions of up to 4.5 °C under the environmental conditions of Coimbatore, India, during February 2020. Karthick et al. [23] investigated the cooling provided by a eutectic PCM based on Zinc Nitrate Hexahydrate and Sodium Sulfate Decahydrate on a tailored semitransparent PV module in Kovilpatti, India, during the year 2018. Measurements showed that incorporating the PCM resulted in instantaneous temperature reductions up to 12 °C, which, over the course of the year, resulted in a relative increase in the electrical yield of 8 %. Furthermore, Singh et al. [24] investigated the effects on the operational temperature of a PV module by attaching one or more conductivity enhancing containers with PCM material (Calcium chloride hexahydrate) on its backside. The authors found that covering the backside of the module with five containers provided much better cooling homogeneity compared to using one single large container. In the experiment, carried in Chennai, India, the authors measured temperature reductions

up to 23.3 °C in the month of June. A two-day experiment in China, carried out by Waqas et al. [25] using RT 24 with limited contact area (0.3 m²) showed a maximum temperature reduction of 9 °C in case of a 50 W PV module. Wongwuttanasatian et al. [26] used palm wax on containers with different layouts (grooved, finned and tubed), finding that the finned option provided the best cooling performance.

The promising potential of thermally managing PV module temperature with PCM has expanded to PVT systems as well. Choubineh et al. [27] focused on an air-cooled PVT system, Rajaei et al. [28] that studied the combination of PCM with thermo-electric generators to cooldown PVT systems using paraffin wax with alumina powder, demonstrating a 12.3 % increase in electrical efficiency in comparison to a water-cooled PVT system. Klugmann-Radziemska and Wcislo-Kucharek [29] conducted a comprehensive set of experiments that consisted of testing three different PCM materials (Paraffin, RT22 and Ceresin) on PV and PVT modules on both laboratory and natural conditions. The authors concluded that the combination of paraffin and water cooling provided the best results but argued that using just the PCM was a suitable solution to provide significant cooling.

The abovementioned literature is only a fraction of the amount of experimental and computational research done investigating PCM implementation in PV systems. For a broader overview, readers are referred to the review work of Ali [30], Biwolde et al. [31], Dutil et al. [32], Huang et al. [33], Kant et al. [34], Khanna et al. [35], Tao et al. [36], and Preet [37].

This work presents a detailed long-term experimental study on the cooling potential of PCM when integrated onto PV modules carried out in multiple locations under two different installation layouts: building integrated and standard rack mounted. The work was carried out for almost two years in Delft, in the Netherlands, and six months in Catania, Italy. The following section presents the materials used and the methodology deployed to undertake the long-term measurements. Section 3 presents the experimental results from both locations, displaying the relationship between the cooling potential provided by the chosen PCM and its effect on the electrical performance of a PV module with respect to the installation layout and the environmental conditions. Section 4 discusses the obtained results and elaborates on the outlook for future research. Section 5 concludes this work.

2. Experimental overview

2.1. Phase change material selection

The experimental works mentioned in the introductory section of this document are usually limited to days up to a maximum of a year (in only one reported work) or indoor testing. No works study a multiannual multiple location test of a single type of PCM under different installation layouts. This work aims to provide insight into how a single type of PCM can provide cooling to PV modules working under the conditions of a BIPV system and a standard rack-mounted system in two climates. For the BIPV layout, the selected location was Delft, in the Netherlands. This location has a moderate annual global horizontal irradiance of 2.95 kWh/m² per day and an annual average ambient temperature of 10.8 °C [38]. BIPV systems are more likely to present higher operational temperatures than their rack-mounted counterparts in this location. Thus, cooling options are an attractive approach to BIPV systems. For the standard rack-mounted layout, the selected location was Catania, Italy. The location has a significantly higher average annual global horizontal irradiance of 4.82 kWh/m² per day and a higher annual average ambient temperature of 17.9 °C [38]. Here the higher solar resource means that PCMs are attractive in potentially increasing large power plant yields. Additionally, the data collected from both layouts is valuable for future modeling efforts.

The selected PCM compound was *calcium chloride hexahydrate*, with references CSP1900/CSP1575, which contain the same compound and melting temperature but differ in the case size. The numbers indicate the

Table 1
Physical and thermal properties of the selected PCM (from Ref. [40]). *Data for the casing of the PCM.

Property	Value
Dimensions (mm)	$(2 \times 157.5 + 190) \times 570 \times 13$
Type of filling	CaCl ₂ ·6H ₂ O
Mass (kg)	1.8
Density (kg/dm ³)	1000
Melting temperature (°C)	26
Latent heat (kJ/kg)	310
Thermal conductivity (W/mK)	1.0
Kinematic viscosity (m ² /s)	9.6×10^{-6}
Thickness* (mm)	0.6
Heat transfer coefficient* (W/mK)	0.5

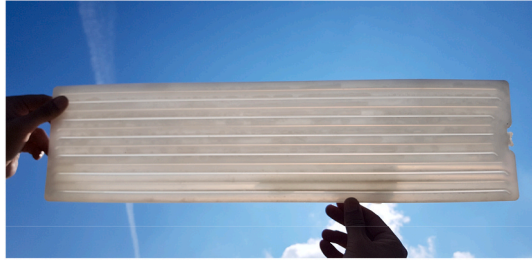


Fig. 1. Selected Phase change material (PCM) encapsulated in a crystal storage panel made of high-density polyethylene. The panel is divided into 6 sections to avoid mixture separation.

width of the casing, thus CSP1575 is 15.75-cm wide and CSP1900 is 19-cm wide. These sizes were selected to fit the active area of the manufactured PV modules, as will be explained later. The main properties of the substance can be found on [Table 1](#). The selected melting temperature of this PCM is 26 °C, with the purpose of testing if under changing environmental conditions, the PV module could be (temperature wise) controlled to perform close to standard test conditions (STC). The mixture is liquid and contained in a polymer casing in the shape of slabs with several grooves to avoid premature separation of the mixture, thus increasing the useful life of the PCM (see [Fig. 1](#)). The manufacturer of the PCM is Orange Climate Autarkis [39].

2.2. Module manufacturing and PCM integration

Providing efficient thermal management to a PV module endowed with a PCM requires the entire active area of the module to be in contact with the selected PCM. The manufacturing of two small PV modules followed the abovementioned condition. Each module consists of sixteen IBC SunPower Maxeon® Gen II solar cells [41] connected in series. The encapsulation materials were a PV glass sheet of 60 cm × 60 cm, 0.5-cm

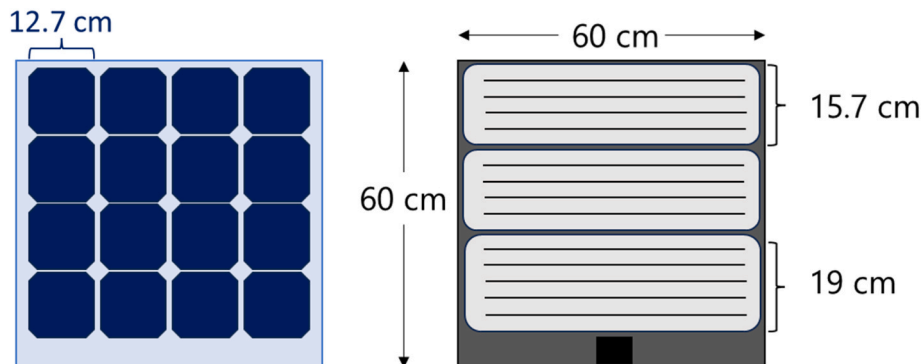


Fig. 2. Layout of the manufactured PV module to ensure that the PCM slabs can be in contact with the entire active area of the PV module to secure optimal cooling: (left) front and (right) rear view of the PV-PCM module.

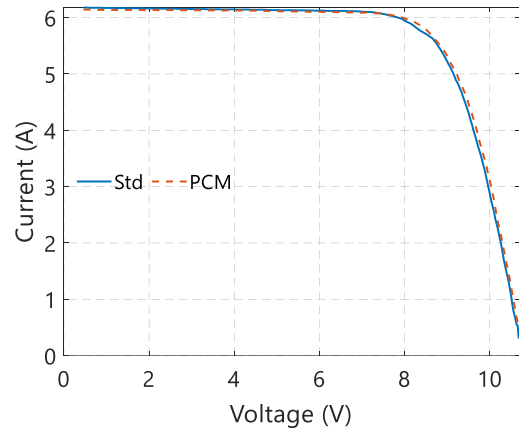


Fig. 3. IV curves of the PV modules manufactured based on 16 IBC Maxeon Gen II solar cells connected in series.

thick ethyl vinyl acrylate (EVA) and a 0.3-cm thick black PET back sheet. The complete layout of the module and the manufactured device are presented in [Fig. 2](#).

To ensure that differences measured within the field experiments are due to the addition of the PCM, the current-voltage (IV) curves of both modules were characterized using a class AAA large area steady state solar simulator (LASS). Additionally, electroluminescence (EL) tests allowed to check the quality of the manufacturing, thus avoiding potential unexpected performance differences due to interconnection issues or cracks that might become worse as the module operates continuously. The result of the former is presented in [Fig. 3](#); while the latter can be found in [appendix D](#). The electrical performance of both modules was found to be almost identical, with differences in power production under standard test conditions of 0.2 %. The EL test showed that none of the modules had manufacturing differences that could produce different performance behavior. The measured electrical parameters of the manufactured modules used in this work is presented in [Table 2](#).

Full details of (i) the experimental setups used at both locations, (ii) the equipment used and (iii) the data validation methodology can be found in [appendices A-C](#) of this document.

Table 2
Electrical parameters of the manufactured PV modules.

Parameter	Standard	PCM
V_{OC} (V)	10.80	10.70
I_{SC} (A)	6.05	5.95
P_{mpp} (W)	48.70	48.60
η (%)	19.90	19.80

3. Experimental results

The experiments carried out at both locations had differences in their installation layout due to the environmental conditions of each location. Also, the number of measured variables were not the same due to technical differences between the facilities. The results from the measurements are therefore presented in two separate sections. Firstly, we explore (i) the cooling that can be provided to a PV module by mechanically attaching PCM slabs on both locations, as well as (ii) the effect on it due to the environmental conditions and the installation layout of the PV module. Secondly, the effect on the electrical performance for each case.

3.1. Cooling potential provided to the PV module by the phase change material under different environmental conditions and installation layouts

3.1.1. Delft – photovoltaic modules with insulated backside

Temperature measurements carried out in Delft consisted of monitoring the values sensed by T-Type thermocouples behind the six chosen solar cells, as shown in Fig. 4(a). The purpose of this placement is to analyze if a homogeneous temperature profile could be obtained in the PV module just by mechanically attaching the PCM slabs. The temperature data was recorded from July 2019 to February 2020. Due to a technical failure of the temperature measurement setup, from that point onwards, it was only possible to monitor electrical parameters.

The construction of temperature profiles for each module allows the analysis of the extent to which the PCM slabs can provide thermal management across the cells within the module. The profiles shown below belong to the moment at which, each month, the standard PV module reaches its highest temperature. For the sake of brevity, only the profiles measured during the two warmest months are displayed in this document.

Fig. 5(a) presents the temperature profile of the standard PV module during the month of July 2019. The highest recorded value of temperature in this month was 78.69 °C in cell 3 (see Fig. 4(a) for reference). The remaining cells presented temperature values no lower than 73.53 °C (cell 2). Overall, the highest temperature difference between the cells within the standard PV was 5.16 °C. At this same time, the PV-PCM module had a temperature profile as shown in Fig. 5(b). The outer cells (1, 2, 5 and 6) registered temperatures substantially lower than their counterparts in the standard module, with the biggest difference measured at cell 5, of 9.62 °C. The cells located in the middle (3, 4), however, had a higher value of temperature compared to 1, 2, 5 and 6. Cell 4 had a temperature difference of only 0.77 °C compared to the same cell of the standard module, very close to the uncertainty of the thermocouple (± 0.5 °C), whereas cell 3 presented a difference with respect to its counterpart in the standard PV module of 5.37 °C. Possible

reasons for this inhomogeneity are explained in the next section.

Fig. 6 presents the same difference on the temperature profile for both modules at the highest recorded temperature in the standard PV module during the month of October 2019. For the case of the standard PV module (Fig. 6(a)), the temperature profile follows the same pattern as the month of July, with cell 3 presenting the highest value (52.72 °C) and cell 2 the lowest (48.16 °C), meaning a maximum temperature difference between the cells of 4.56 °C.

Fig. 6(b) presents the temperature profile of the PV module with attached PCM slabs. At this moment in October 2019, the behavior of the PV module remains consistent with that of July. The outer cells present the lowest measured temperatures, whereas those in the middle registered the highest values. The difference between the warmest (cell 4 with 42.51 °C) and the coldest (cell 6 with 35.49 °C) cell in this month at this time is 7.02 °C, which is consistent with the difference observed during July (6.83 °C). The PV module with the PCM attached always presents the largest gradient in its temperature profile, with cells 3 and 4 consistently being the warmest.

Comparison between the profiles presented in Fig. 6(a) and (b) indicates that the PCM slabs can provide substantial thermal control of the PV module. Cells 5 and 6 present temperature reductions of 14.92 °C and 15.38 °C, respectively. The figures presented above only showcase the moment when the standard PV module reaches its highest temperature. The behavior of both modules during these days is shown in Fig. 7(a) and 8(a) for July 2019 and October 2019, respectively, which depict the average temperature (mean measured value of cells 1–6) per hour. During July 30th, the PCM slabs managed to reduce the average temperature of the PV module until 16:00 h compared to the standard case. After 17:00 h, the lowering ambient temperature and irradiance cooled down both modules. However, since the PCM slab presented the phase change (solid-to-liquid), the reverse process released the stored heat, which in turn warmed up the PV module, as it is seen later that day around 19.00 h. During October, the 17th, the PCM slabs provided more consistent thermal management, and the PV module with the slabs attached only presented higher operational temperatures after 17:00 h.

The temperature difference between the average value measured from the six thermocouples on each PV module is denoted henceforth as ΔT , and mathematically defined as:

$$\Delta T (^{\circ}\text{C}) = \overline{T_{PV-PCM}} - \overline{T_{PV-Std}} \quad (1)$$

Negative values of ΔT indicate that the PCM slabs thermally manage the PV module compared to the standard case. A positive value indicates that the module with the PCM slabs presents a higher operational temperature than the standard one. Fig. 7(b) presents the calculated value of ΔT for every time instant, grouped per hour of the day, and its relationship with the measured plane of array irradiance during the entire month of July 2019. The color code indicates the hour in which the PCM

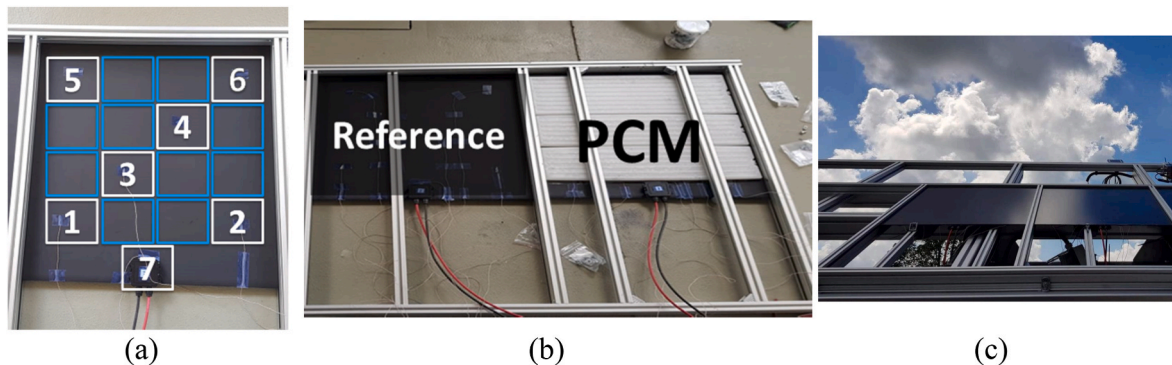


Fig. 4. (a) Placement of the thermocouples on each of the manufactured modules; each square represents a solar cell within the PV module. The 7 thermocouples were attached using thermal tape. (b) The use of a tailored-made aluminum frame allowed mechanically attaching the PCM slabs on the backside of the PV module. (c) Both PV modules were installed on a fixed rack, oriented south, with a tilt angle of 35°. For clarity, in picture (c), cells 5 and 6 are the furthest from the base of the mounting rack.

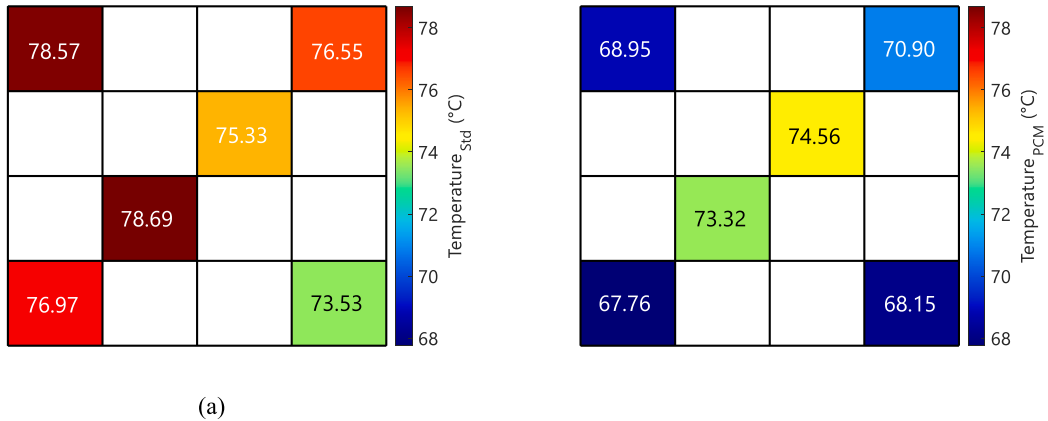


Fig. 5. (a) Temperature profile of a standard PV module at the highest value of temperature recorded during July 2019 in Delft. The squares describe the solar cell within the module following the same distribution and numbering presented in Fig. 4(a). The largest difference between the measured temperatures for this module was 5.16 °C. (b) Temperature profile of a PV module endowed with PCM slabs mechanically attached to its backside (PV-PCM module) for the same period as the case of (a). The largest difference between the values of the measured temperatures in this case was 6.83 °C. The limits for the color graph were selected based on the lowest value of temperature recorded on (b) and the highest value recorded on (a).

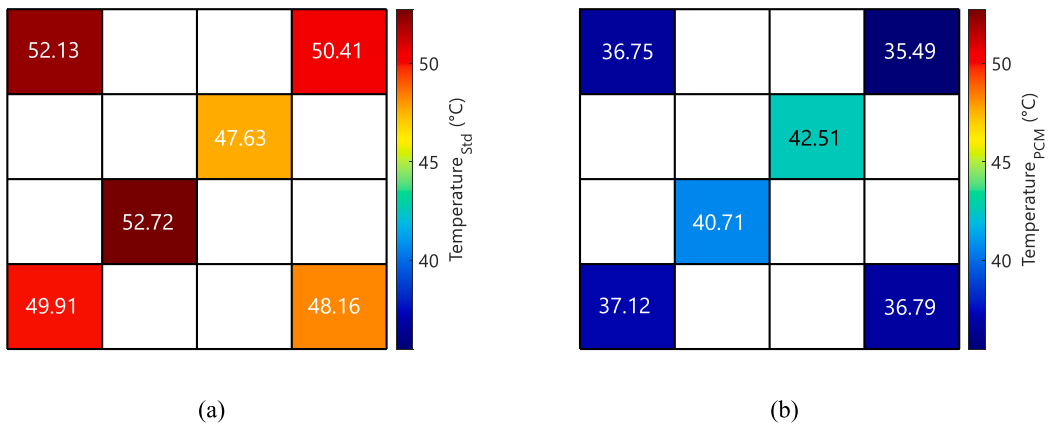


Fig. 6. (a) Temperature profile of a standard PV module at the highest value of temperature recorded during October 2019 in Delft. The squares describe the solar cell within the module following the same distribution and numbering presented in Fig. 4(a). The largest difference between the measured temperatures for this module was 4.56 °C. (b) Temperature profile of the PV-PCM module for the same period as the case of (a). The largest difference between the values of the measured temperatures in this case was 7.02 °C. The limits for the color graph were selected based on the lowest value of temperature recorded on (b) and the highest value recorded on (a).

slabs provide cooling to the PV module (blue towards greens and yellows) and those in which that PV module presented a higher value of temperature compared to the standard one (orange toward reds). The overall trend for the month follows that presented for the single day of the month at Fig. 7(a), where most of the cooling is provided around noon until 15:00 h. From 9:00 to 10:00 h, particularly at high values of G_{POA} , the PCM provides cooling that reduces the operational temperature of the PV module consistently between 10 °C and 15 °C. This effect is significantly lost later in the day, reaching a warming effect that produces a temperature difference of up to 5 °C more often observed after 17:00 h. Fig. 8(b) indicate that for the month of October, the PCM provides more consistent cooling to the PV module through most of the day, particularly at the hours of high values of recorded G_{POA} . However, in Fig. 8(b) we note that during October, high values of G_{POA} were around 20 % lower compared to July, leading to comparatively lower operating temperatures on both modules. Nevertheless, the maximum temperature difference registered in terms of cooling was like that in July, of 15 °C. The warming effect, on the other hand, was higher during October, with measured differences up to 10 °C. These higher temperatures, however, only occurred at low values of G_{POA} late in the day.

The thermal control provided by the PCM greatly depends on the amount of irradiance reaching the PV modules, as shown in Figs. 7 and 8, but other environmental conditions also contribute to the effectiveness of the PCM slabs. For this analysis, the average value of the temperature measured by the sensors on both modules was divided into calendar seasons. Summer of 2019 for example, covers the data ranging from July 24th (starting of the measurements) until September 21st. For autumn, the dates used were from the 22nd of September until 21st of December. Lastly, winter encompasses the remaining data (measured until February 8th, 2020). Fig. 9 presents the histograms of the average recorded PV module temperature for summer (Fig. 9(a)) and autumn (Fig. 9(b)) for both the standard module and the PV-PCM module. To avoid overpopulating the data, a filter discarded hours at which the value of G_{POA} was below 100 W/m² for each case. A different limit was set for the measurements of winter, whose results are presented in the appendix.

During summer, the average temperature reduction provided by the PCM slabs to the PV module was 6.24 °C. The calculated mean temperature on the standard module for this season was 44.76 °C, compared to 38.52 °C for the case of the PV-PCM module. During autumn, the

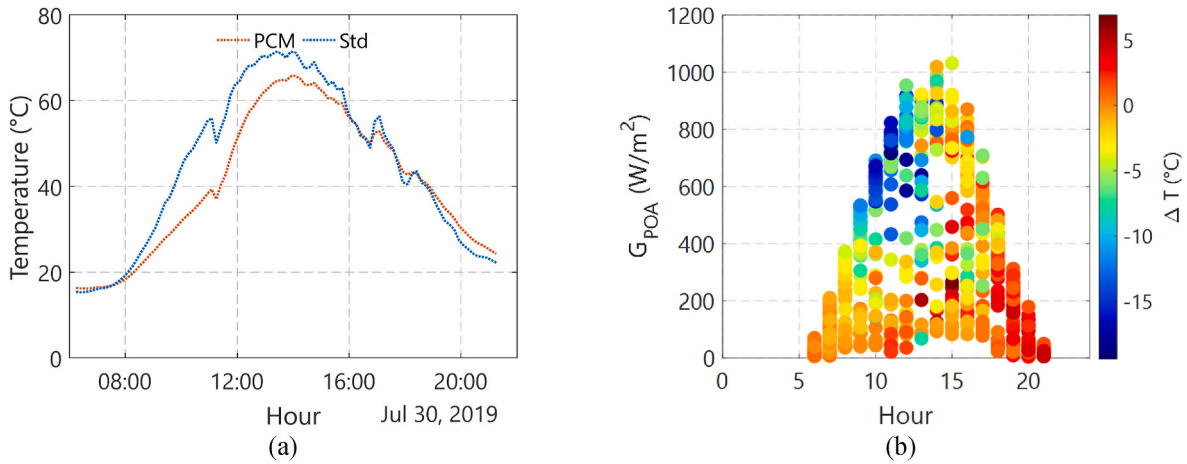


Fig. 7. (a) Hourly average operational temperature of a PV module with (PCM) and without (Std) PCM slabs mechanically attached on the backside for a summer day in Delft. The PCM effectively reduces the operational temperature of the PV module with an insulated backside, particularly from the morning until early in the afternoon. Once the phase change takes place, and the ambient temperature starts cooling down, the release of heat from the PCM slabs keep the modules at a higher temperature compared to its standard counterpart. (b) Hourly average temperature difference between the standard PV module and the PV-PCM module related to the plane of array irradiance (G_{POA}) for the month of July. From 10 a.m. until noon, the PCM slab can reduce the operational temperature of a PV module up to 15 °C. The cooling effect reduces overtime and after 15:00 h the PV-PCM module presents higher operational temperature compared to the standard one.

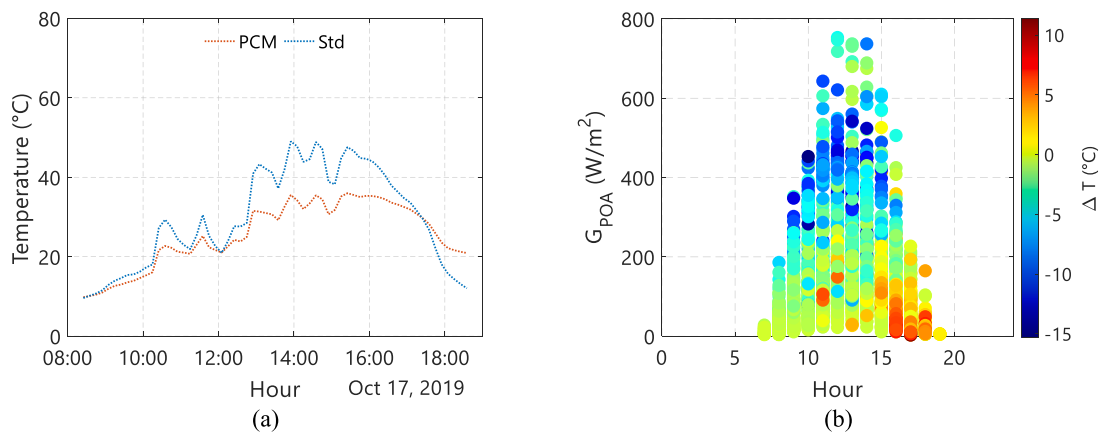


Fig. 8. (a) Hourly average operational temperature of a PV module with (PCM) and without (Std) PCM slabs mechanically attached on the backside for an autumn day in Delft. Under this conditions, the PCM manages to provide cooling for most of the day. The phase change is not completed and the PCM module only presents a higher value of operational temperature compared to the standard case at 17:00 h. (b) Hourly average temperature difference between the standard PV module and the PV-PCM module related to the plane of array irradiance G_{POA} for the month of October. The lower values of G_{POA} compared to July (see Fig. 7(b)) allow the PCM slabs to provide sufficient cooling capacity for almost the entire day to the PV module they are attached to.

mean recorded temperature on the standard module was 20.43 °C, whereas the PV-PCM module had a mean temperature of 18.34 °C, representing a temperature reduction of 2.09 °C. For these two seasons, the average value of the recorded ambient temperature was 21.40 °C and 11.75 °C, respectively.

Fig. 10 provides information on how the value of ΔT changes in relation with environmental factors. Fig. 10(a) presents the relationship between ΔT , ambient temperature and G_{POA} during the summer of 2019 in Delft. The best cooling (denoted by blue to yellow colors) is provided at values of G_{POA} greater than 400 W/m² and lower values of ambient temperature, particularly when these are below the melting temperature of the chosen PCM slabs (26 °C). Nevertheless, the PCM slabs still manage to provide cooling at high ambient temperatures. The warming effect occurs mostly late in the day, when the density of red dots becomes more noticeable. The effect of wind speed and G_{POA} is presented in Fig. 10(b), which indicate that the best cooling is achieved at low values of wind speed (below 3 m/s) and high values of G_{POA} . It is important to highlight that in Delft, the backside of both PV modules

was completely insulated. Higher wind speeds provide better cooling by convection mechanisms. An insulated backside reduces the effectiveness of convection, creating a more advantageous scenario for the PCM. However, even under this installation layout, high values of wind speed reduce the effectiveness of the PCM compared to the standard case, but the values of ΔT remain negative. Fig. 10(c) presents the relationship between ΔT , wind speed and ambient temperature. In this case, the lowest values of ΔT are distributed mostly at low values of wind speed (below 3 m/s) and values of ambient temperature below the melting temperature of the PCM slab. Ultimately, the effect of these environmental factors is not as acute as that of G_{POA} , as Fig. 10(d) shows. During the summer of 2019, the PCM slabs were able to reduce the operating temperature of the PV module for most of the day, with the most reductions seen before 15:00 h.

Fig. 11 presents the same analysis of Fig. 10 but for a colder season, autumn. The lower values of G_{POA} and ambient temperature compared to summer help the PCM slabs to provide cooling for a wider range of values of G_{POA} . Particularly, this was because the measured ambient

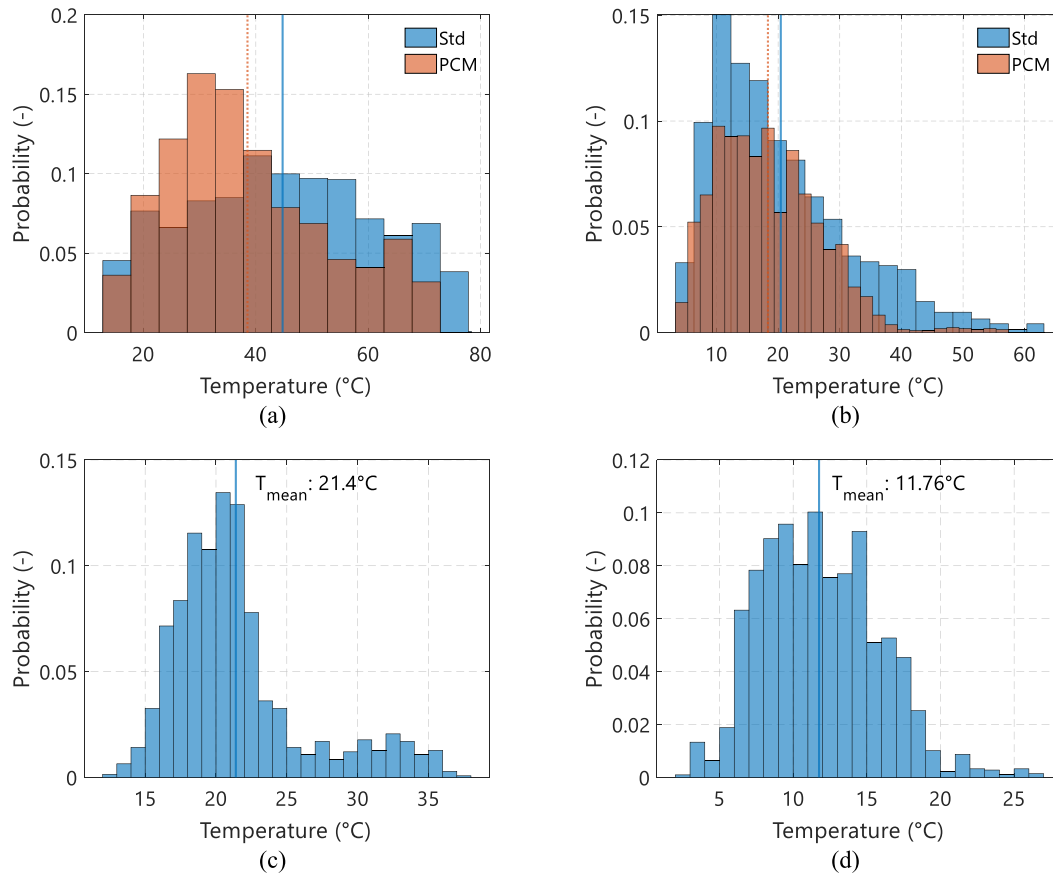


Fig. 9. (a) Histogram of the measured operational temperature of the standard PV module (Std) and the PV-PCM module during the summer of 2019 (July 1 – September 21, 2019) between 10:00 and 17:00 h. The vertical lines indicate the mean value of the measured temperature. During these hours, the PV-PCM module presented a mean measured value of **38.52 °C (dashed line)**. Compared to the value measured on the standard PV module (**44.76 °C, continuous line**), the PCM provides an average temperature reduction of 6.24 °C. (b) Histogram of the measured operational temperature of the standard PV module (Std) and the PV-PCM module during the autumn of 2019 (September 21 – December 21, 2019) between 10:00 and 17:00 h. As presented in (a), the mean values of temperature for the PV module with and without PCM are depicted by the vertical lines. (c) Complementary to (a), histogram of the measured ambient temperature for the summer of 2019, showcasing a mean value of 21.40 °C. (d) Complementary to (b), histogram of the measured ambient temperature for the autumn of 2019, with a mean value of 11.76 °C.

temperature values for this season were seldom above the melting point of the PCM. Notice that in Fig. 11, as opposed to Fig. 10, the color coding is slightly different. In the latter case, cooling was indicated by blue to orange colors, while warming was indicated by red colors. In Fig. 11, cooling is indicated by blue to green, whereas warming is indicated by yellow to red. This is because, during this season, the warming effect from the PCM slabs was higher compared to the summer, mostly due to lower measured ambient temperature during the evening. During solidification, the heat transferred from the PCM slabs to the PV module maintains the temperature of the latter at significantly higher values than its standard counterpart, which cools down much faster due to the low values of ambient temperature. The warming effect, however, occurs at times when its impact on the overall electrical efficiency of the module is relatively low, as will be presented in the following section. During autumn, the measured values of wind speed were higher when compared to the summer, but high wind speed occurred at hours of low G_{POA} , as shown in Fig. 11(b). Also, during the autumn, the overall effect of ambient temperature and wind speed was not as significant as the effect produced by G_{POA} . Fig. 11(c) indicates that during this season the values of ΔT that indicate better cooling happened at ambient temperatures lower than the melting temperature of the PCM, even during high wind speeds. Very low values of ambient temperatures and high values of wind speed resulted in a slight warming effect that never surpasses 5 °C. As in the case of summer, G_{POA} remains the most significant

parameter (see Fig. 11(d)). During autumn, the cooling potential provided by the PCM slabs had better consistency throughout the day compared to the summer.

3.1.2. Catania – photovoltaic modules with open backside

The experimental setup used in Catania contained the same standard and PV-PCM modules as those used in Delft. However, the methodology differs on the following aspects: (i) the PCM slabs were mechanically attached to the backside of the same PV module used for this purpose in Delft, but the backside of both modules was not insulated; (ii) the temperature of each module was measured utilizing one PT100 thermal sensor that was attached at their geometrical center. Lastly, the recorded electrical parameters were the maximum power point voltage (V_{mpp}) and maximum power point current (I_{mpp}) as opposed to the full IV curves measured in Delft. Results from the electrical measurements for each location are discussed in section 3.2.

Fig. 12(a) presents the hourly operating temperature of both standard and PV-PCM modules during a day in January 2023 in Catania, Italy. Over the day, the operating temperature of the PV-PCM module is lower than that of the standard module. At around 14:00 h, the standard module starts to cool down at a considerably higher rate than the module with the PCM. As a result, from 14:00 onwards, the overall effect from the PCM slabs is that of warming up of the module. As for the case of Delft, using the ΔT metric allows to assess the cooling provided by the

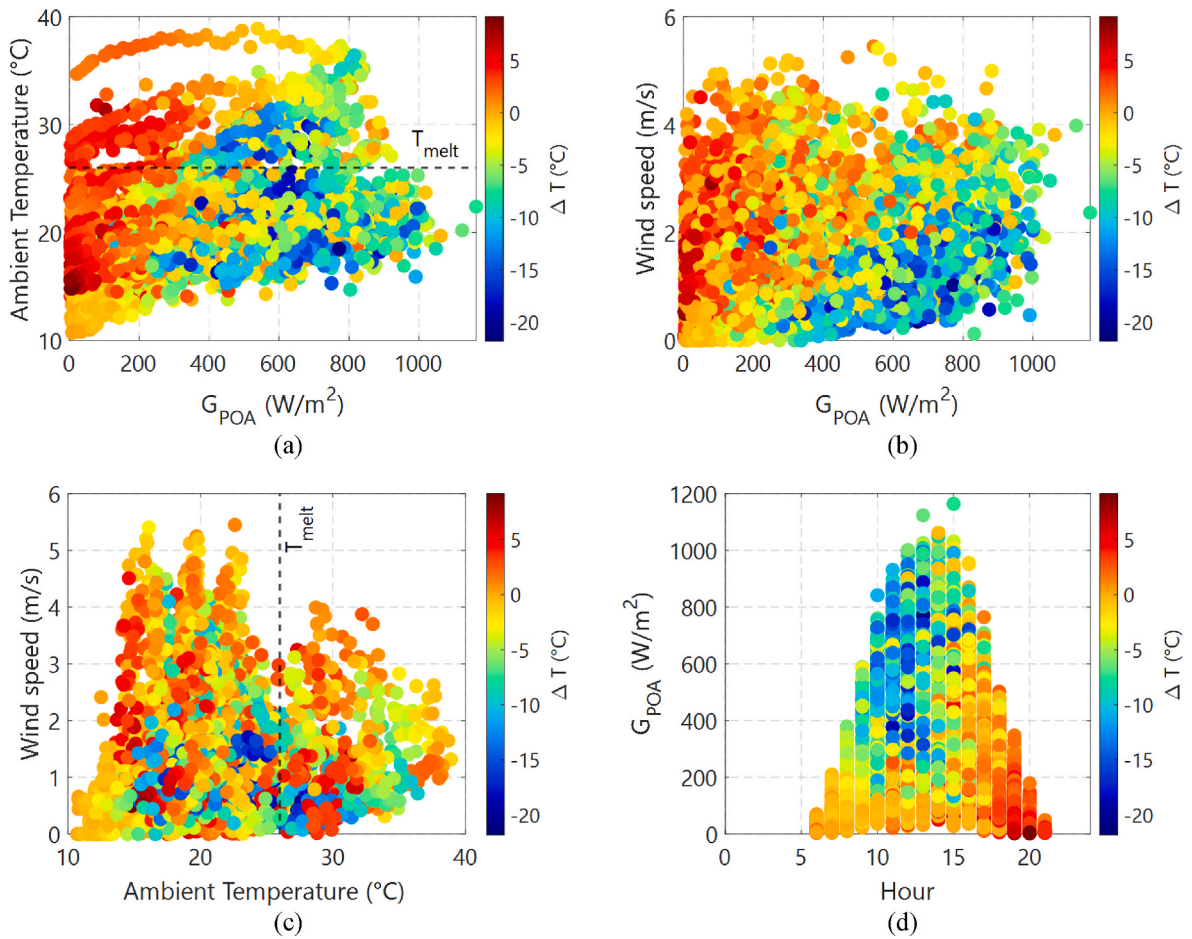


Fig. 10. Influence of environmental conditions on the average temperature difference ΔT ($^{\circ}\text{C}$) between PV-PCM and standard modules during summer 2019 in Delft: (a) effect of the ambient temperature related to the plane of array irradiance. The value of the melting temperature T_{melt} of the PCM is denoted by the dashed line and equal to $26\text{ }^{\circ}\text{C}$; (b) effect of the wind speed related to the plane of array irradiance; (c) effect of the wind speed related to the ambient temperature; and (d) effect of the plane of array irradiance on the hourly temperature difference for the entire season.

PCM. Fig. 12(b) presents the trend on the value of ΔT , per hour, as related to G_{POA} during the month of January. The best cooling happens from the early hours of the morning until 14:00 h. Cooling is guaranteed during most of the hours of high values of G_{POA} . Notice that the limits depicted by the color code go from high cooling (blue, with a limiting value of $-12\text{ }^{\circ}\text{C}$) to high warming (green towards reds, with a limiting value of $15\text{ }^{\circ}\text{C}$). The highest values of warming occur late in the day at low values of G_{POA} , which implies the potential negative effects on electrical performance are mostly avoided.

In Catania, the cooling from the PCM slabs shift towards earlier hours of the day as ambient temperatures start to rise, similar to the behavior observed in Delft. Fig. 13(a) shows that the PV module with the attached PCM slabs has a lower operating temperature compared to the standard case until noon on a day in May 2023. Afterward, the effect produced is a warming up of the PV module until the end of the day. This trend is seen throughout the entire month of May, as seen in Fig. 13(b), where the maximum cooling presents between 9:00 and 11:00 h, with ΔT values as low as $-14\text{ }^{\circ}\text{C}$. During the afternoon, the warming of the module with the PCM can go as high as $10\text{ }^{\circ}\text{C}$ compared to the standard module, and this warming occurs at G_{POA} values above 400 W/m^2 , which leads to electrical performance losses.

From a seasonal standpoint, in Catania, both during winter and spring, the average value of temperature for the PV-PCM module is higher than the value measured on the standard module. Fig. 14(a) and (b) shows the histograms of the measured temperatures for both modules during winter and spring, respectively. The values were filtered to

those measured between 10:00 and 17:00 h, which is the time frame at which high values of G_{POA} happen. During the months of winter in Catania, the PV-PCM module had a mean measured temperature $2.72\text{ }^{\circ}\text{C}$ higher than the standard module with mean temperature values over the period of $26.98\text{ }^{\circ}\text{C}$ against $24.26\text{ }^{\circ}\text{C}$, respectively. During spring, with measurements done between the 21st of March and the May 16, 2023, the PV-PCM module also had a higher mean measured temperature ($3.04\text{ }^{\circ}\text{C}$) compared to that of the standard module ($31.64\text{ }^{\circ}\text{C}$ vs $28.60\text{ }^{\circ}\text{C}$, respectively). These generally higher mean temperatures at module level are correlated with higher mean ambient temperature measured in Catania during spring ($4.52\text{ }^{\circ}\text{C}$ higher than during winter), as shown in Fig. 14(c) and (d).

Since the backside of both PV modules was left without insulation (as opposed to the experiments carried out in Delft), it is of interest to analyze how the environmental conditions impact, for this installation layout, the cooling potential provided by the PCM slabs. Given that most of the measurements done in Catania were during the winter season (52% of the data points), Fig. 15 shows how the value of ΔT changes in relation with environmental factors. Fig. 15(a) presents the relationship between G_{POA} , ambient temperature and ΔT . An important aspect of this case is that the ambient temperature never had a value above the melting temperature of the PCM ($26\text{ }^{\circ}\text{C}$). Given this condition, the cooling potential provided by the PCM (and represented by blue hues) increases with the value of G_{POA} . There are, however, instances in which a warming effect was measured (represented by green to red hues) even at high G_{POA} values.

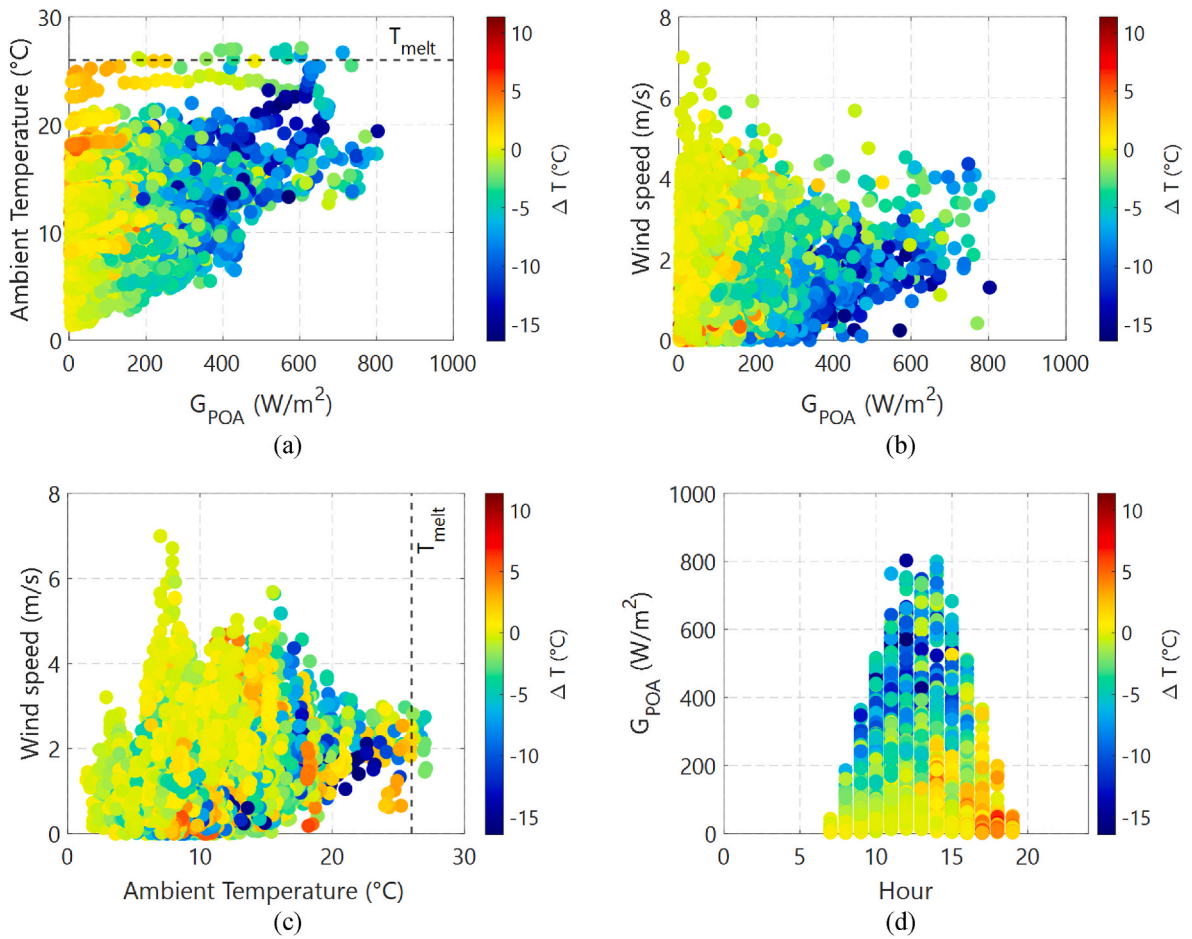


Fig. 11. Influence of environmental conditions on the average temperature difference ΔT ($^{\circ}\text{C}$) during autumn 2019 in Delft: (a) effect of the ambient temperature related to the plane of array irradiance. The value of the melting temperature T_{melt} of the PCM is denoted by the dashed line and equal to 26°C ; (b) effect of the wind speed related to the plane of array irradiance; (c) effect of the wind speed related to the ambient temperature; and (d) effect of the plane of array irradiance on the hourly temperature difference for the entire season.

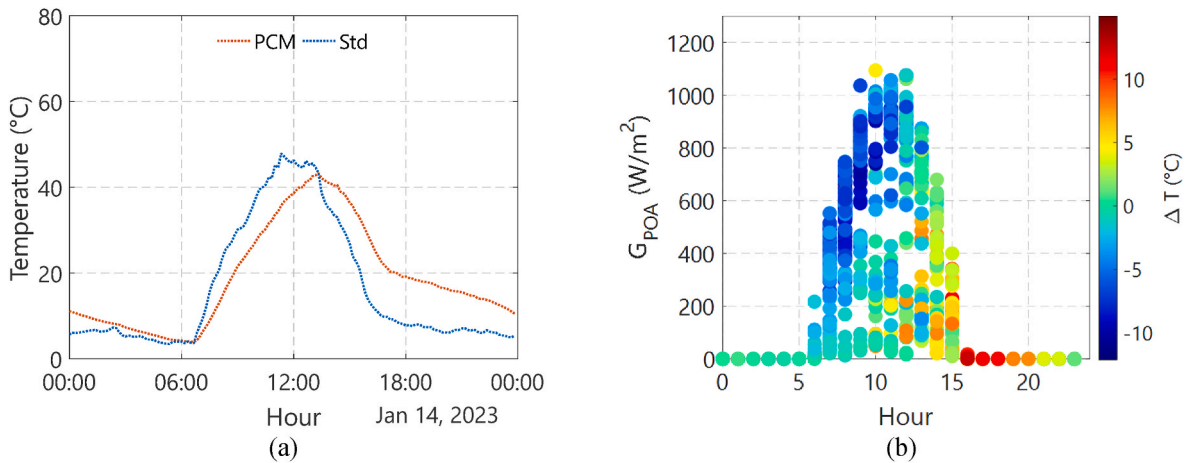


Fig. 12. (a) Hourly operational temperature of the PV module with (PCM) and without (Std) PCM slabs attached to the backside with an open backside during a day in January 2023 in Catania, Italy. (b) Hourly average operational temperature difference for the entire month of January between the PV-PCM module and the standard counterpart. The PCM slabs allow the reduction of the temperature of the PV module consistently until 14:00 h, covering the time of the highest irradiance values.

The relationship between G_{POA} , wind speed conditions and ΔT is illustrated in Fig. 15(b). The best cooling provided by the PCM slabs is generally present at low values of wind speed for a wide range of irradiance conditions. Nevertheless, even at high values of wind speed and

high values of G_{POA} , the PCM slabs still provide significant cooling. Most of the warming effect occurs during the afternoon hours as shown in Fig. 15(d), which implies that the PCM is already saturated, and the warming effect occurs. High windspeed values during this time increase

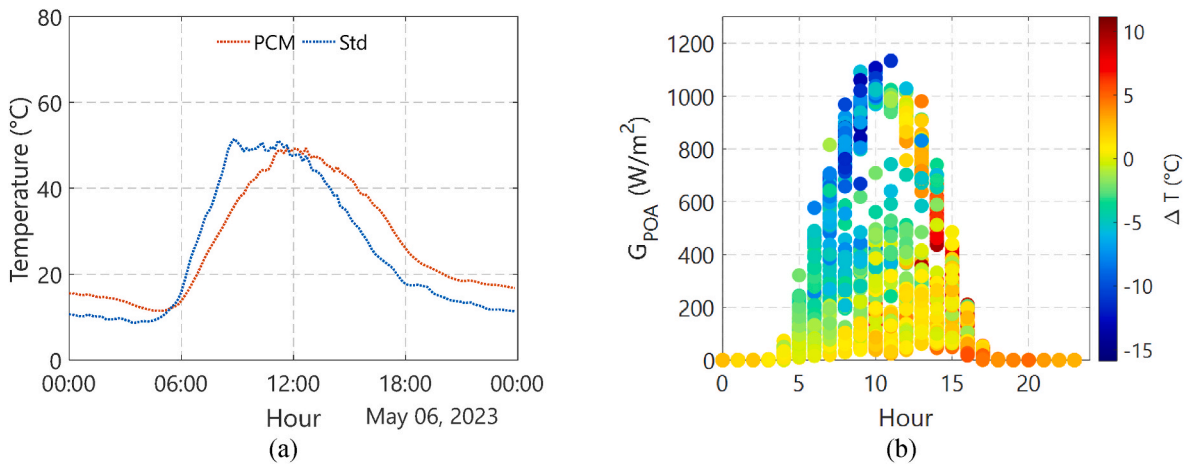


Fig. 13. (a) Hourly operational temperature of the PV module with (PCM) and without (Std) PCM slabs attached to the backside with an open backside during a day in May 2023 in Catania, Italy. (b) Hourly average operational temperature difference for the entire month of May between the PV-PCM module and the standard counterpart. The PCM slabs allow the reduction of the temperature of the PV module consistently until 10:00 h, covering some of the highest irradiance values.

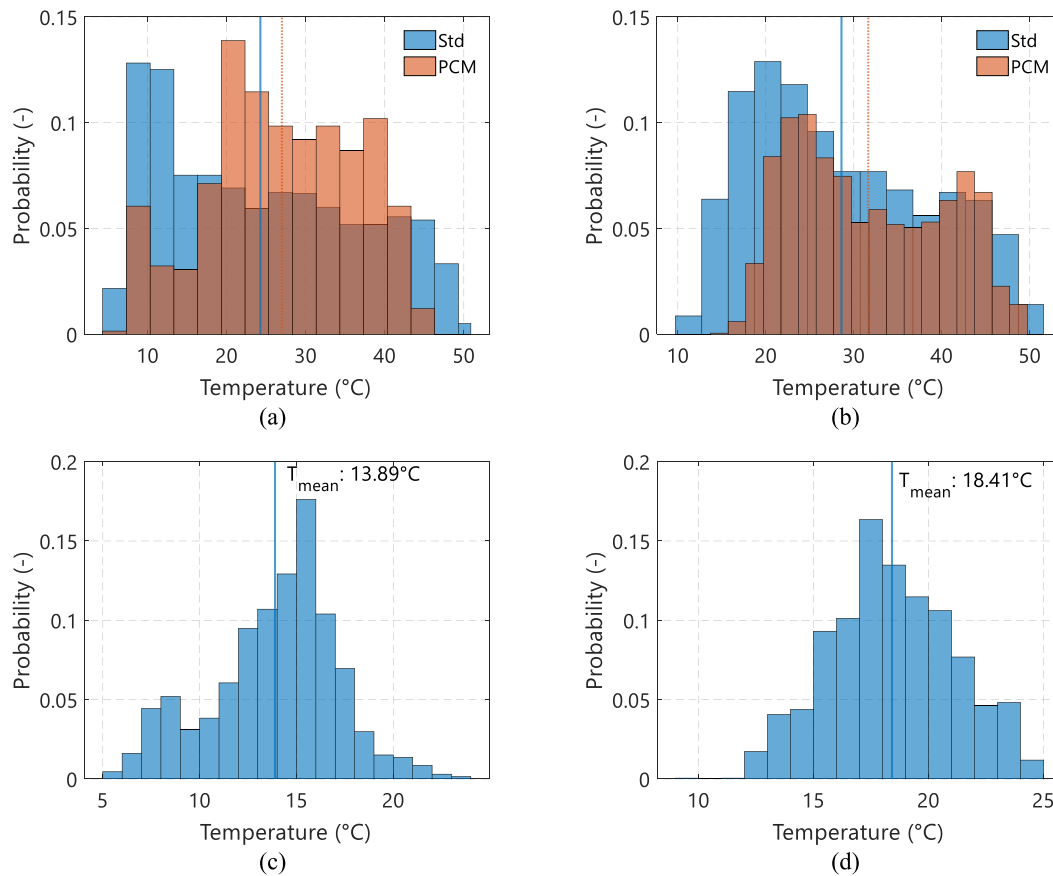


Fig. 14. (a) Histogram of the measured operational temperature of the standard PV module (Std) and the PV-PCM module during winter 2023 (January 13 – March 21) between 10:00 and 17:00. The vertical lines indicate the mean value of the measured temperature. During these hours, the PV-PCM module is warmed up by the PCM, presenting a mean measured value of 26.98 °C (dashed line), 2.72 °C higher than that of the standard PV module (24.26 °C, continuous line). (b) Histogram of the measured operational temperature of the standard PV module (Std) and the PV-PCM module during the beginning of spring 2023 (March 21 – May 16) between 10:00 and 17:00. As presented in (a), the mean values of temperature for the PV module with and without PCM are depicted by the vertical lines. (c) Complementary to (a), histogram of the measured ambient temperature for the same period, showcasing a mean value of 13.89 °C. (d) Complementary to (b), histogram of the measured ambient temperature for the spring of 2023, with a mean value of 18.41 °C.

the value of ΔT towards positive values, but its influence is less significant than that of ambient temperature. Due to the very low ambient temperature, which never exceeded the melting temperature of the

PCM, very little can be deduced from its relationship to wind speed and ΔT (see Fig. 15(c)).

The ambient temperature remained stable within the first two

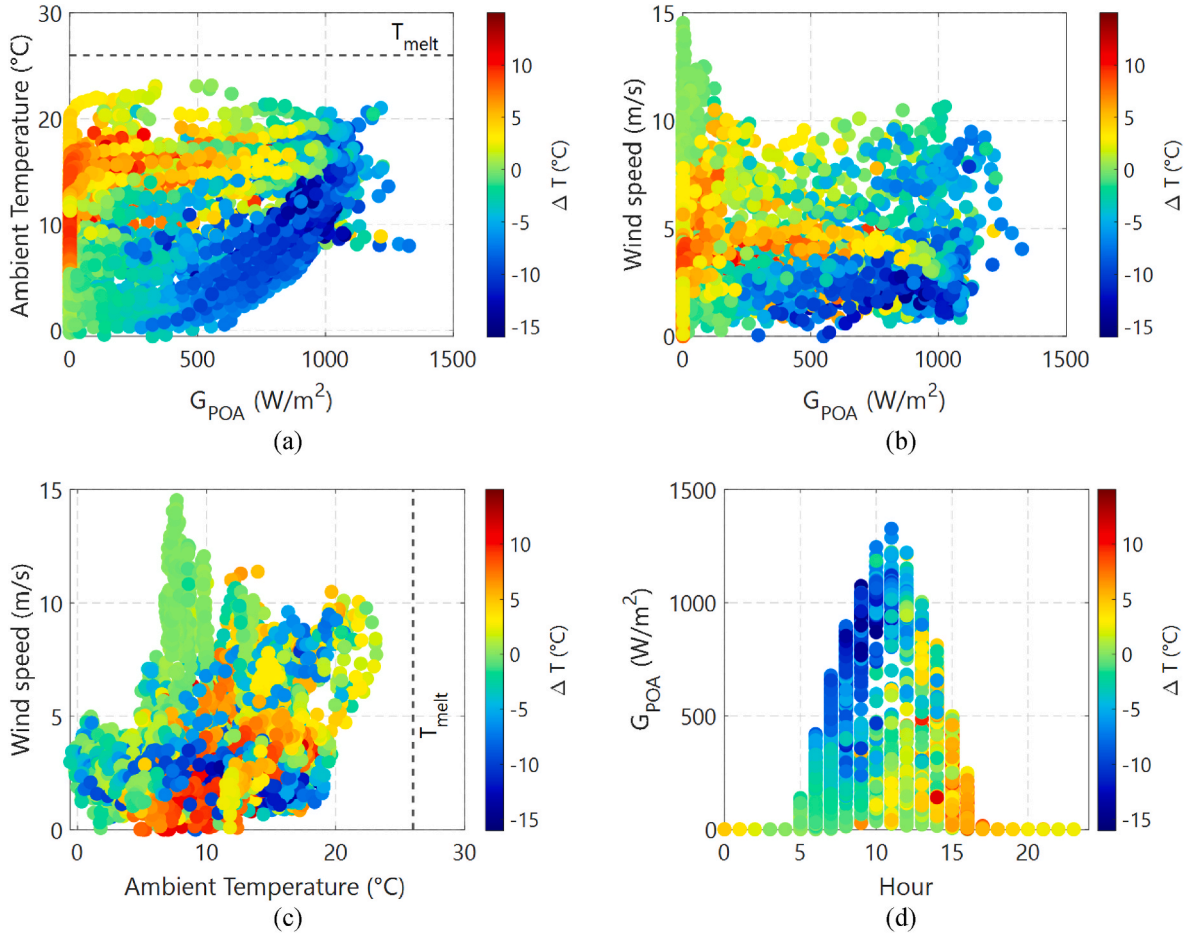


Fig. 15. Influence of environmental conditions on the average temperature difference ΔT ($^{\circ}\text{C}$) during the Winter of 2023 in Catania, Italy. (a) Effect of the ambient temperature related to the plane of array irradiance. The value of the melting temperature T_{melt} of the PCM is denoted by the dashed line and equal to 26°C ; (b) Effect of the windspeed related to the plane of array irradiance. (c) Effect of the windspeed related to the ambient temperature. (c) Effect of the plane of array irradiance on the hourly temperature difference for the entire season.

months of spring (March through May), so the overall relationship between ΔT and the measured environmental parameters remained very similar to that of winter, as shown in the supporting information.

3.2. Effects of a PCM on the electrical performance of a PV module

As explained in [appendices A and B](#), both locations were equipped with devices that were able to monitor the electrical performance of both modules during the experiments. The instantaneous power produced by the modules was recorded, and the data was synchronized with the remaining parameters (weather conditions, operational temperature, etc.). The data presented in this section is already filtered using the methods explained in [appendix C](#).

The PCM slabs, located on the backside of one of the PV modules, do not produce any optical loss. Its only effect is the reduction of the operating temperature by using the heat extracted from the module to create a phase change at a constant temperature. The main effect of this reduction is measured by an increased operating and open circuit voltage of the module, and a slight reduction in its current production. This latter effect, however, is much lower than the former, and the overall result is an increased efficiency in electrical power production.

Given the measured electrical parameters, the calculation of ΔP , defined as the difference between the instantaneous power produced by the standard module and that produced by the PV-PCM module, is mathematically expressed as follows:

$$\Delta P (W) = P_{PV-std} - P_{PV-PCM} \quad (2)$$

ΔP serves as a figure of merit to analyze the overall effect of the PCM in the electrical performance of a PV module in a similar way to its effect on operating temperature presented in the previous section. A **negative** value of ΔP implies that the module with the PCM slabs is producing **more** power than its standard opposite, whereas a **positive** value of ΔP means that is producing **less** power.

Due to technical difficulties, maintenance procedures and other scheduled activities carried out during the experimental work done in Delft, it was not possible to continually monitor the power production of the PV modules. As a result, some months have significantly more data than others. Reduction of potential biases regarding monthly energy yield calculations is done by calculating the energy production per hour measured in a month, which is defined as χ_{DC} and mathematically expressed as:

$$\chi_{DC} \left(\frac{W \cdot h}{hr - month} \right) = \frac{1}{N} \sum P_{PV} \quad (3)$$

Where N is the number of hours in which energy production was reliably measured on each month. The value of χ_{DC} is estimated separately for each module and the relative energy gain or loss δ_{DC} is calculated as:

$$\delta_{DC} (\%) = \left(\frac{\chi_{PV-PCM} - \chi_{PV-std}}{\chi_{PV-std}} \right) \cdot 100 \quad (4)$$

The data presented based on the calculations done using Equation (2) to Equation (4) has a time resolution of 5 min for the case of ΔP and monthly, for the case of χ_{DC} and δ_{DC} .

3.2.1. Delft: photovoltaic modules with insulated backside

The thermal control provided by the PCM causes a lower decrease in voltage compared to the standard case. Fig. 16(a) presents the measured open circuit voltage (V_{OC}) of both modules during the same day of July as presented in Fig. 7(a). The V_{OC} value of the PV-PCM module remains higher compared to the standard module until 17:00 h. This is the same time at which thermal control is lost and the warming effect starts. From this time of the day onwards, the warming effect from the PCM slabs produces a lower value of V_{OC} on the module. This, however, happens at a time at which G_{POA} is low, and consequently, the value of ΔP becomes slightly positive, meaning that the standard module produces slightly more power (<1 W) than the PV-PCM. This occurs on almost all instances of the summer, as showcased by Fig. 16(b), where most of the hours of the day with high value of G_{POA} the PV-PCM module presents higher power output.

The thermal management provided by the PCM slabs during the summer of 2019 is maintained during the summers of 2020 and 2021 as shown in Fig. 17(a) and (b), respectively. In both years, negative values of ΔP are achieved during most of the hours at which G_{POA} is above 600 W/m². Only occasionally, during these hours, ΔP has a positive value. Notice that, as expected, the behavior observed in Fig. 16(b) and 17 follow that of Fig. 10(d): the best observed improvements in electrical performance happen when the PCM slabs provide substantial temperature reduction.

Regarding normalized energy yield, as defined by χ_{DC} , the PV-PCM module always had a higher value compared to the standard module. Even during the cold months of November and December, with limited solar resource, the PCM slabs manage to provide an overall positive effect, as shown in Fig. 18(a). The relative gain, expressed by δ_{DC} , is presented in Fig. 18(b). Relative gains during this year range from 1 % in December to 4 % in September.

Data for eleven months of 2020 indicates that implementation of PCM slabs provides increased energy yield production under all seasonal conditions, with the winter months of December and February indicating the lowest relative gain (see Fig. 19(a) and (b)). During the spring and summer months, the relative gain ranges from 2.1 % to 2.6 %, which are lower values compared to 2019. During 2021, the relative gain was much more stable across all the months, ranging from 2.1 % to 2.6 % from January towards July, as presented by Fig. 19(c) and (d).

The variance in the relative gain observed in the PV-PCM module can be attributed, mainly, to the number of hours in which the modules worked during each month. For example, in July 2019, a total of 141.25 h were recorded on both modules. During August, it was only possible to

measure the electrical parameters for 56 h. Given the dependence of the thermal management provided by the PCM on environmental factors, particularly irradiation, fewer hours of measurement can bias the relative gain in a positive or negative way. An example of each case is September 2019 (with 63 h of measurements) and February 2020 (with 27 h of measurements) where the gain is unusually high and unusually low, respectively. The months that had a substantial number of measurements were April, May, August, September 2020 and March, April, and June 2021 with measured hours ranging from 500 to 650 per month. During these months, the relative gain is always estimated between 2.1 % to 2.5 %, thus providing a good indicator of the overall monthly performance benefits provided by the PCM slabs.

3.2.2. Catania, Italy: photovoltaic modules with open backside

In Catania, the combination of high values of G_{POA} and low values of ambient temperature results in a power production gain in the morning and a power production loss in the afternoon when comparing the measurements of both modules and calculating ΔP , as depicted in Fig. 20(b). These changes in gain and loss of power from the PV module with PCM slabs compared to the standard module are caused by the effects on voltage produced by changing temperature (see Fig. 20(a)).

In Delft, the value of ΔP was maintained negative during most of the day during summer. In Catania, this was not observed even during the winter months, where some losses were present just 2 h after noon. One possible explanation for this observation is that the open backside of the standard PV module allows for rapid cooling, aided by low ambient temperature and better convection mechanisms. On the PV-PCM module, low ambient temperatures can cause a reversal of the phase change, meaning that heat might be transferred from the slabs toward the module at earlier hours. Additionally, the presence of the slabs with low or no phase change rate reduces the effectiveness of convection mechanisms on the backside of the module, which hinders their cooling compared to the standard case.

Despite this, during the five months of measurements conducted in Catania, the overall effect of implementing the PCM slabs produced gains in the electrical energy yield of the PV module going from 1.3 % in January to 1.6 % in February (see Fig. 21(a)). The relative gains, however, are smaller than those measured in Delft. Like in the case of the experiment in Delft, it was not possible to monitor the electrical parameters during the entirety of the months, so the gains presented in Fig. 21(b) are an initial indicator of the relative potential benefits and results might vary for a setup measured for longer periods.

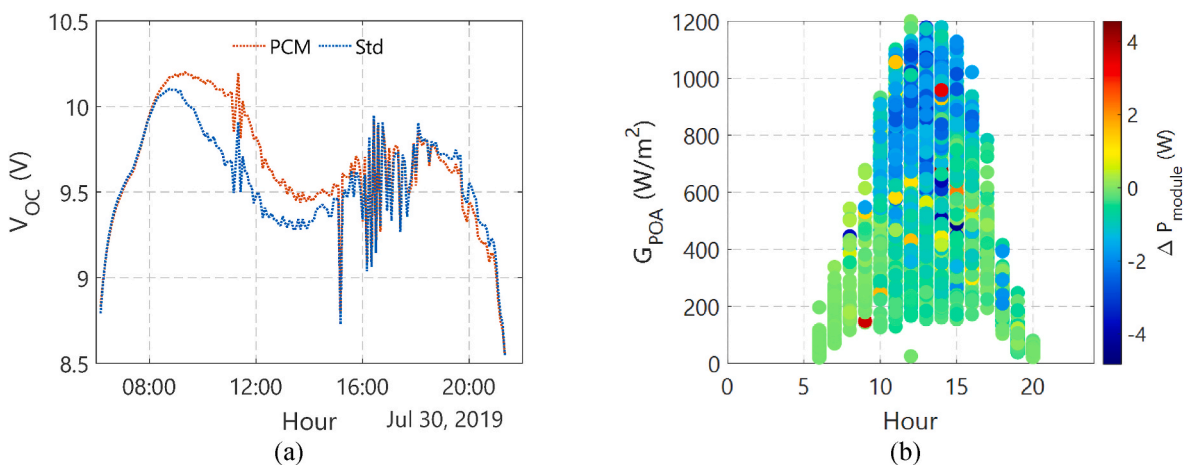


Fig. 16. (a) Measured open circuit voltage of two PV modules, one with PCM slab attached on the backside (orange line) and a standard PV module during a day in July 2019 in Delft, Netherlands. In both cases, the backside of the PV modules was insulated with a 19-mm thick Armaflex® slab. (b) Difference in electrical power produced ΔP , as defined by Equation (2), per hour during the summer season (July–September 2019) in Delft. A negative value of ΔP means that the PV-PCM module produces more electrical power than its standard counterpart. This definition was decided to follow a similar color code as that presented to analyze the cooling potential in the previous section.

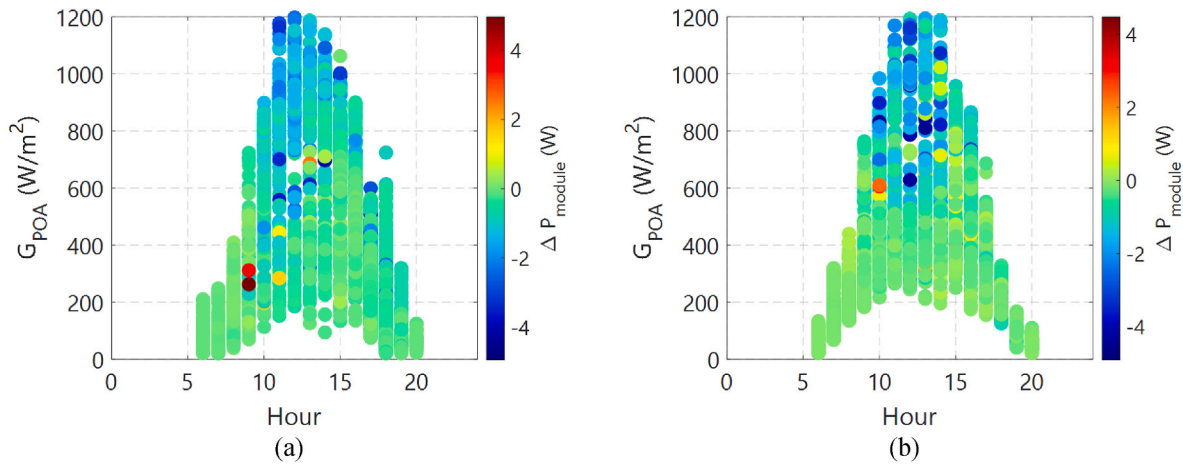


Fig. 17. (a) Difference in electrical power produced ΔP , as defined by Equation (2), per hour for the summer season (July–September 2020) in Delft. A negative value of ΔP means that the PV-PCM module produces more electrical power than its standard counterpart. (b) The same relationship as presented in (a) but for the summer of 2021 in Delft.

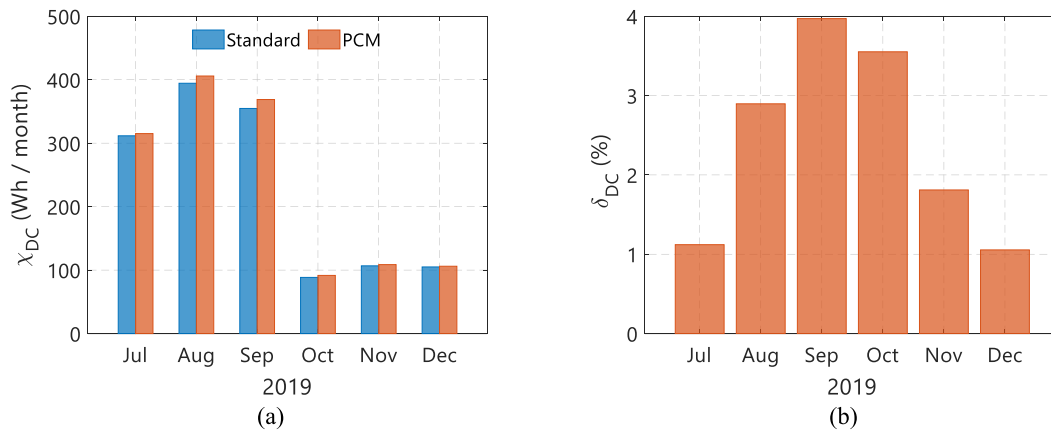


Fig. 18. (a) Monthly values of χ_{DC} as defined by Equation (4), which represents the sum of energy divided by the number of working hours during the month for each PV module. (b) Relative gain δ_{DC} demonstrates that the PCM slabs provided positive energy yield effects during all the measured months of 2019.

4. Discussion

From the data presented in the previous section, the following points of discussion are salient.

4.1. Cooling mechanisms, cooling potential and temperature homogeneity

Once the PCM is mechanically attached to the backside of the PV module, the produced heat travels through the polymer encapsulation to the salt hydrate, which is in the solid phase. The initial heat transfer governing mechanism is conduction. A thin layer of the solid PCM increases its temperature until it reaches its melting temperature, and then the *charging* phase change begins [42]. As the PCM melts, the viscous forces begin to be surpassed by buoyancy forces [43], and a combination of conduction-convection governs the heat transfer. The liquified PCM starts flowing since the liquid phase of the PCM has a lower density than the solid phase, so the flow drifts upwards. Once the flow hits the upper surface of the casing, it is then directed to the boundary interface between both phases, increasing the melting rate by creating convection cells. Under these conditions, the governing heat transfer mechanism is natural convection. As the melting fraction of the PCM increases, the melting rate declines, and the process enters the shrinking solid regime [44]. Once the melting fraction reaches near unity, the thermal energy from the PV panel keeps being stored in the liquid PCM as sensible heat

[45]. Solidification occurs when heat starts being extracted from the PCM due to cooling of the PV panel and a reduction of the environmental temperature. During solidification, the governing heat transfer mechanism is almost exclusively conduction, since the thermal conductivity of the solid phase is higher than the liquid phase [46–48].

The time it takes to fully melt the PCM is dependent on many factors. The nature of the PCM itself, for example, determines its thermal conductivity, cinematic viscosity and thermal diffusivity, and hence its Prandtl number. On materials with high Prandtl number the melting is limited by the thermal transport, whereas those with low Prandtl number, the melting process is limited by their mass transport [44]. Furthermore, the geometry, orientation and tilt angle also impact the time required to fully melt the material. For the case of rectangular casings, decreasing the tilt angle from fully vertical (90°) towards fully horizontal (0°) increases the time it takes to melt the PCM [49,50]. Likewise, the presence of internal fins [51,52] and the addition of nanoparticles [53,54] can speed up the melting process by increasing the heat transfer performance.

The selected PCM slabs provides a substantial cooling potential to PV modules just by mechanically attaching them to the backside, with measured reductions of operational temperatures up to -15°C in both locations, which are reductions in the range of those observed in other research work, as summarized in Section 1. The cooling could be provided for extended periods of time. In Delft, for example, the selected

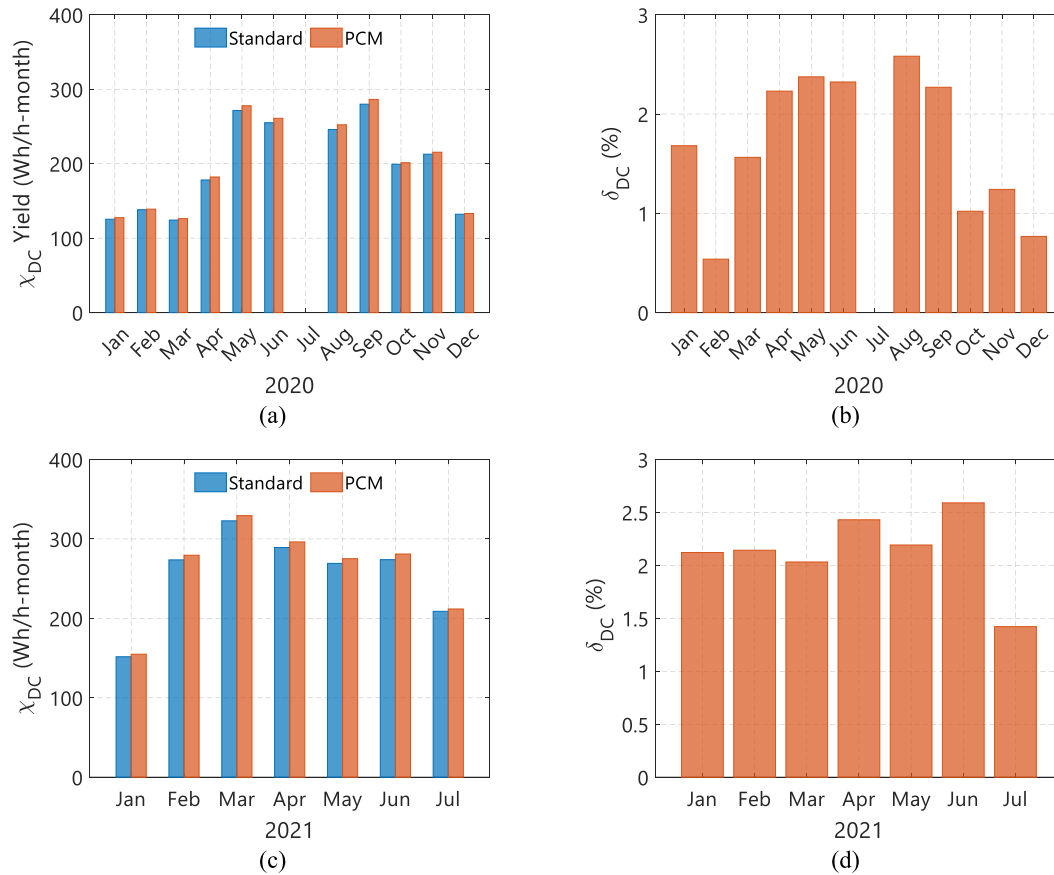


Fig. 19. (a) Monthly values of χ_{DC} as defined by Equation (3), for the year 2020, representing the sum of energy divided by the number of working hours during the month for each PV module. (b) Relative gain δ_{DC} evidence that the PCM slabs provided positive energy yield effects during all the measured months of 2020. Due to a failure in the system, no data was collected during July of this year. (c) Monthly values of χ_{DC} for the year 2021 and (d) relative gain δ_{DC} computed for all the measured months of 2021.

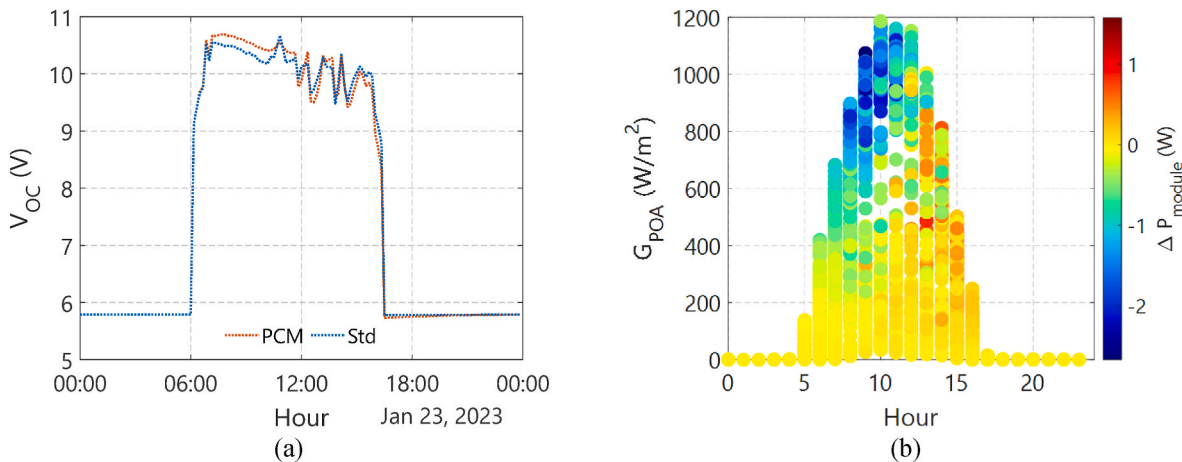


Fig. 20. (a) Measured open circuit voltage of the two PV modules, the PV-PCM (orange dotted line) and the standard PV module (blue dotted line) during a day in January 2023 in Catania, Italy. In both cases, the installation layout was a rack mounted system with no obstruction on the backside. (b) Difference in electrical power produced ΔP , as defined by Equation (2), per hour for winter months of 2023 in Catania. A negative value of ΔP means that the PV-PCM module produces more electrical power than its standard counterpart.

PCM slab could thermally manage the PV module for most of the day, even during the summer season (see Fig. 8(b) and 17). In Catania, thermal control could not be secured throughout the day, even during the winter months of January to March 2023 (see Fig. 15(d)). In the afternoon hours, the module with the PCM slabs had higher measure

temperatures than the standard case. This led to lower comparative voltage values, thus indicating power losses. This shortcoming could be potentially avoided by choosing PCMs with different melting temperatures, depending on the average ambient temperature of the installation location.

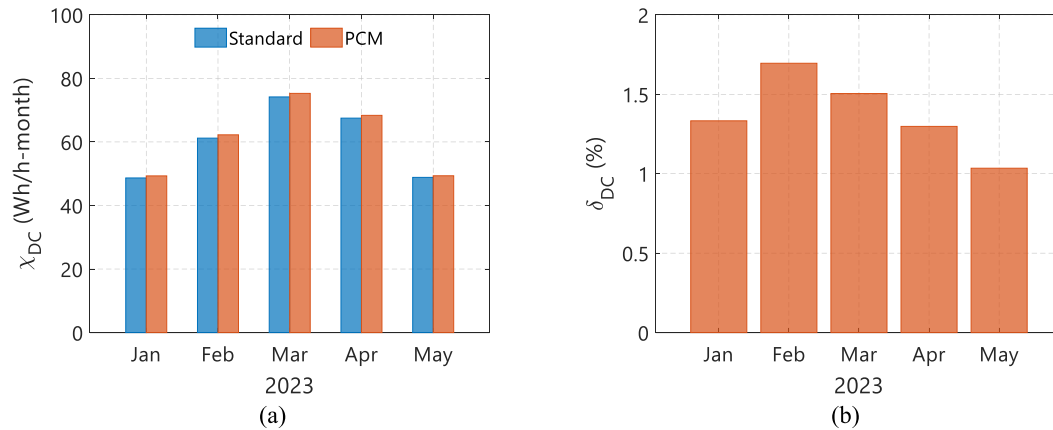


Fig. 21. (a) Monthly values of χ_{DC} , as defined by Equation (3), for the year 2023 in Catania, Italy, representing the sum of energy divided by the number of working hours during the month for each PV module. (b) Relative gain δ_{DC} denote that the PCM slabs provided positive energy yield effects during all the measured months of 2023.

There are, however, potential issues with temperature homogeneity. Figs. 5 and 6 evidence that there is a need to provide better contact from the PCM slabs into the backside of the PV module. The temperature measurements done on the cells at the center of the module had values that differed from those at the edges by an amount larger than their counterparts in the standard PV module. This implies that contact from the PCM slabs on these cells is insufficient for efficient thermal management. The aluminum frame, as shown in Fig. 4(b) provides sufficient contact at the edges, where the cooling from the PCM slabs is measured to be optimal. More options for ensuring sufficient contact need to be investigated.

4.2. Effects of environmental conditions and installation layout in cooling potential and energy yield

Figs. 10, 11 and 15 present the effect of the environmental parameters on the capacity of the PCM slabs to provide cooling (defined by the metric ΔT). The irradiance reaching the PV modules, G_{POA} , and the ambient temperature were found to be the most impacting factors, the former correlates to the findings of Fadl and Eames [43]. Wind conditions had a moderate effect, only negatively affecting ΔT at high values of wind speeds. The ambient temperature of the location is particularly important in relation to the melting temperature of the selected PCM. The best reduction in operating temperature of the PV module happens at conditions of high G_{POA} and ambient temperature lower than the abovementioned melting value. This is consistent with other published experimental work [55]. In both locations, the average ambient temperature is low enough to guarantee most of the phase change happens due to the heat extracted from the PV module.

Delft had the better conditions for the effectiveness of the selected PCM, partly because the backside of both PV modules was insulated. This hinders the cooling ability of the standard module by eliminating the convection heat transfer at the backside, producing higher operating temperatures during high irradiance than in the case of no insulation. The PCM slabs compensated for this by acting as heat sinks working at a much lower temperature. Thus, the instantaneous differences in power production between both modules could be as high as 4.3 W (see Fig. 16(b)) due to higher operating voltage (Fig. 16(a)). Overall, under this installation layout, the PV-PCM module exhibited, on average, between 2.1 % and 2.5 % higher normalized energy yield compared to its standard counterpart, accounting for all the years of measurement (see Figs. 18 and 19).

On the other hand, the warming effect was greater in Catania than the one observed in Delft, occurring also during hours with high G_{POA} . This location not only has on average higher irradiance than Delft, but

also presents on average more frequent clear skies, with a diffuse to global irradiance factor of 0.367 compared to Delft's 0.531 [38]. Even during the low ambient temperatures of winter, the warming effect in the afternoon was greater than the one observed in Delft. A possible explanation for this is the installation layout selected for Catania. With no insulation on the backside, the standard module can cool down more effectively. The PCM slabs provide thermal control if the material is in phase change, otherwise, it will act as an additional thermal resistance that hinders the module's ability to cool down via convection mechanisms at the backside. Additionally, clear skies improve the radiative cooling of the module, as a consequence of this, the standard module begins to cool down quickly (see Fig. 12(a) and 13(a)). The PV-PCM module, under these conditions, starts to act as a heat sink for the PCM that will start to reverse the phase change, causing increased temperatures. In terms of normalized energy yield, the relative gain was estimated ranging from 1.3 to 1.6 %.

Since the cooling potential provided by the PV module is very sensitive to the value of G_{POA} , the optimal melting temperature of the PCM oriented towards PV applications also depends on the tilt and orientation selected for the system. For example, a PV façade oriented towards the west in the northern hemisphere will have the highest values of G_{POA} during the afternoon. Moreover, the values will be lower than modules installed on a south-facing façade. This sensitivity means that a PCM with a lower melting temperature will be more suitable for the modules-oriented west. Optimizing the PCM parameters while considering the installation layout of the PV modules will provide better energy efficiency.

4.3. Technical aspects for implementation

From a technical perspective, the implementation of PCM slabs into PV modules looks straightforward. Significant cooling is possible by mechanically attaching them to the backside. There are, however, the following important considerations to optimize their benefit.

The most important properties for the selection of a PCM material for PV applications are its melting temperature and its latent heat (see the work of Verheijen [56]). The knowledge from manufacturers of tuning these properties is significant, and it is a challenge for the designer to select the most appropriate PCM for its application. As shown in this work, the best matching comes from a clear understanding of the environmental conditions of any given location, and a careful consideration of the installation layout of the PV system. Integrated PV modules on façades, for example, will receive, on average, lower irradiance. A PCM material with a melting temperature higher than the average ambient temperature during the warmest months will provide good

thermal control to the PV modules across the year. For a given PCM material, the latent heat also improves thermal control, but not to the same extent as the melting temperature.

Moreover, the tilt angle also influences the time to melt of the PCM material. A given PCM working under stable conditions, changing the tilt angle from 90° (vertical) towards and horizontal orientation increases the time it takes for the material to change phase [49]. A PCM will melt slower on a façade system during summer in the northern hemisphere compared to one working under a tilted roof due to lower irradiance. However, for the same value of irradiance, the façade PCM will melt faster due to its tilt. Additionally, the casing design of the PCM also impacts its performance. The casing of the product used in this work divides the slab into compartments, which can increase melting rate by creating different buoyancy zones instead of one as depicted in the experiments carried by Kamkari and Shokouhmand [42]. The design, however, differs from the abovementioned study on using grooves instead of fins, so the difference in the overall melting time and temperature profiles compared to a non-grooved casing is yet to be studied. Decreasing the melting time can be counterproductive, as it can translate into fewer hours of thermal control, particularly in the hours of high irradiance. All these aspects need to be studied when designing and implementing PCM materials to provide cooling to PV Systems.

Ensuring effective contact between the PCM slabs and the cells represents a different challenge. The PV modules manufactured for this project were designed so that the entire active area could be covered by PCM slabs. These might not be possible with standard full-cell PV modules, since the junction box is usually located at the back of one or two cells. This condition makes it impossible to cover the active area with PCM slabs. However, half-cell PV modules usually have their junction box in the middle of both groups of cells, without covering any active area. For these modules, PCM slabs are a particularly good option to provide thermal control.

Added weight is another important technical aspect regarding the PCM slabs used in this study. The addition of these devices can significantly increase the overall weight of the modules. Adding ten PCM slabs will increase the weight of the setup by 20 kg, which might become problematic for roof or façade installations. The high-density polymer (HDP) casing is designed to avoid mixture separation and leakage, ensuring higher reliability. *Orange Climate Autarkis* tested the abovementioned PCM products via the standardized test done by the RAL Quality Association PCM [57] (test RAL-GZ 896). The results, according to the company, proved that the slabs can sustain more than thirty thousand cycles of work. For a PV application that has one cycle per day, this number of cycles are translated into more than 80 years of service.

From an economic perspective, the addition of PCM slabs does not represent a substantial increase in the overall price of the PV system. *Orange Climate Autarkis* company estimates that depending on economy of scale and packaging, costs of the PCM slabs could be in the range of 2€/kg to 6€/kg.

Reducing the operational temperature not only increases the electrical performance of a PV module but also has important benefits related to reliability. For example, simulation work has predicted that a reduction between 2 and 3 °C in the operational temperature of a PV module can extend its lifetime by two years in hot climates and just one year in moderate ones [8]. PCM slabs, with its better cooling performance, have the potential of improving the lifetime further, the extent of which is out of the scope of this work but will be studied in the future. Furthermore, during the evening, the cooling of the PV module is slower due to the warming provided by the solidification of the PCM. This behaviour could reduce the daily thermal gradient, which is the difference between the highest and the lowest operating temperature of a PV module on a given day. This thermal gradient also impacts the reliability of the PV module [58–60]. Studying this potential benefit can further increase the interest and economic viability of the implementation of these devices on PV systems.

5. Conclusions

This work presents a long-term study of the effect of adding phase change materials onto a 48.60 W_p PV module under different installation layouts and locations. It compares its performance to a 48.70 W_p PV module working under the same conditions but without PCM. The selected compound provided by *Orange Climate Autarkis* (phase change: solid-to-liquid) was Calcium Chloride Hexahydrate. The material was encased in high-density polymer within slabs and had a melting temperature of 26 °C with a latent heat of 300 kJ/l. The selected locations were Delft, in the Netherlands, with moderate climatic conditions, frequently overcast days, and varied irradiation throughout the year. Measurements in this location started in 2019 and finished in 2021. Due to technical challenges and maintenance activities, the data collection was non-continuous, obtaining 4314 h of operation after that filtering was applied to the collected data to ensure its quality. The second location was Catania, Italy. A location with frequent clear skies and high irradiance, even during winter. In this location, the experiments carried out during the winter and early spring months of 2023 allowed the measurement of 1220 h of operation with a resolution of 10 min. In Delft, both modules were insulated on the backside to mimic the condition of a building-integrated system. In Catania, the modules were kept with their backside open, thus representing the condition of a standard rack-mounted system.

Results from the experiments showed that the PCM slabs could provide significant operational temperature reductions to the PV module consistently. Under the tested building integrated layout in Delft, for example, during all the measured summer months of 2019, 2020, and 2021, the PV-PCM module presented temperature reductions of up to 15 °C compared to the standard module. Moreover, thermal management was possible during most of the sunny hours in the summer days, with an average temperature reduction of 6.24 °C. The trend continued through the months of autumn, where the average temperature reduction was 2.09 °C, primarily due to the lower irradiance available during that period. Overall, the PCM provided thermal control during the sunny hours of all the seasons measured.

In Catania, the trend was like that observed in Delft for the standard rack-mounted layout. However, the warming effect was more impactful due to the combination of lower ambient temperatures and high irradiance values. In the abovementioned conditions, the standard module cools down quite rapidly late in the afternoon, aided by clear skies. The heat stored on the PCM starts to transfer to the PV module when the reverse phase change happens (liquid-to-solid), thus warming the module. On average, the PV-PCM module in Catania presented an average operating temperature slightly higher than its standard counterpart, by 2.72 °C in winter and 3.04 °C at the start of spring.

During all the measured months in both locations, the PCM slabs provided sufficient thermal control to increase the energy yield of the PV module compared to the standard case. In Delft, the relative yield gain, normalized per hour of operation, was between 2.1 and 2.5 % during the months with more recorded data. The benefit could be around 1 % or 4 % on months with less data, thus highlighting the importance of long-term continuous experimental work to have a fair assessment of the potential benefits of PCM. In Catania, the benefit provided by the PCM was lower than that measured in Delft, with a relative increase in the normalized energy yield ranging between 1.3 and 1.6 %.

The environmental parameters that affect the ability of the PCM to provide cooling are the combined effects of irradiance and ambient temperature. Under high ambient temperature and high irradiance conditions, the PCM transitions quickly, thus reducing the time in which thermal control is achieved. Afterward, the PV-PCM module begins to present higher operational temperatures than its standard counterpart. Selecting a PCM with a higher melting temperature or latent heat value can reduce this condition. However, this could hinder potential benefits in colder months. Therefore, it is necessary to perform a detailed analysis of the conditions at which a PV system will operate to select an

appropriate PCM that ensures benefits under all conditions. Smith et al. [61] provide valuable insight into this matter.

CRedit authorship contribution statement

Juan Camilo Ortiz Lizcano: Writing – original draft, Visualization, Methodology, Investigation, Formal analysis, Data curation, Conceptualization. **Hesan Ziar:** Writing – review & editing, Supervision, Funding acquisition, Formal analysis, Conceptualization. **Cas de Mooij:** Methodology, Investigation. **Mario P.F. Verheijen:** Methodology, Investigation. **Chris van Nierop Sanchez:** Methodology, Investigation. **Davide Ferlito:** Supervision, Data curation. **Carmelo Connelli:** Supervision. **Andrea Canino:** Writing – review & editing, Supervision. **Miro Zeman:** Supervision. **Olindo Isabella:** Writing – review & editing, Supervision, Funding acquisition, Conceptualization.

Declaration of competing interest

The authors declare the following financial interests/personal relationships which may be considered as potential competing interests:

Juan Camilo Ortiz Lizcano reports financial support was provided by Horizon 2020 European Innovation Council Fast Track to Innovation. Juan Camilo Ortiz Lizcano reports equipment, drugs, or supplies was provided by Orange Climate Autarkis. If there are other authors, they

Appendix

A. Experimental work carried out in Delft, Netherlands

Both modules were mounted onto a measurement rack located at the monitoring station of Delft University of Technology (see Fig. 4(c)). The premises are equipped with two measuring racks, a dual axis tracking rack, and a manual rack. The latter allows the selection of any desired azimuth for a fixed tilt and was selected for the experimental work. The rack has a 35° tilt and was oriented towards South. Once the PCM slabs were mechanically attached to the backside of the PV module, a 19-mm thick Armaflex® slab was adhered to each module, simulating an insulating backside condition frequently encountered in building integrated solutions.

For the temperature measurement, 21 T-type thermocouples from RS components were calibrated by placing them inside an insulated chamber that was heated up to a value of 27 °C. Seven thermocouples were attached to each module using 3M™ thermally conductive adhesive transfer tape (8805); six of them were located behind selected solar cells and the seventh placed close to the junction box. The selected distribution of the temperature sensors is shown in Fig. 4(a). Manufactured aluminum frames provided the attachment of the modules on the monitoring rack, and the attachment of the PCM slabs to the back of the PV module, as shown in Fig. 4(b).

Temperature measurements were recorded using a Picolog® datalogger and a Raspberry Pi device at 30-s intervals from July 2019 until February 2020. Electrical parameters were monitored and stored from July 2019 until August 2021. Other environmental parameters measured were ambient temperature, wind speed, global horizontal, diffuse horizontal and direct normal irradiances (GHI, DHI and DNI, respectively). Table A1 provides information on the measured variables, the related instruments, technical characteristics and uncertainty σ of the measurements. For the case of the measured electrical power, the uncertainty is estimated using the following equation:

$$\sigma_p = \sqrt{\left(\frac{\delta P}{\delta V} \cdot \sigma_v\right)^2 + \left(\frac{\delta P}{\delta I} \cdot \sigma_l\right)^2} \quad (\text{A1})$$

The measured data was initially filtered with a resolution of 5 min since the instruments could have differences in the time at which their respective measurement was recorded. Furthermore, potential outliers and erroneous data were filtered out by using a two-diode model of the selected PV modules. The measured values of plane of array irradiance (G_{POA}) and module temperature (T_{PV}) were used as inputs for this model and later compared to the measured electrical parameters of both PV modules. Any large deviation was considered an outlier and eliminated from the data. More details on this procedure can be found in the appendix. In total, 30 % of the raw data measured during 2019 was filtered, 24 % for the case of the data measured during 2020 and 15 % from the one measured during 2021. Figure A1 presents the results for both the standard PV module (blue circles) and the PV module with the PCM slabs (orange squares). The data presented belongs to measurements where the value of G_{POA} was greater than 20 W/m². The power correlates with the value of G_{POA} linearly with almost no outliers, indicating a good quality in the selected data.

Table A 1 Measured variables at the monitoring station in Delft, Netherlands. Irradiance on the plane of the array (G_{POA}), PV performance parameters and measurement of other environmental parameters were carried out using the LPVO MP1010F-1 [62]

declare that they have no known competing financial interests or personal relationships that could have appeared to influence the work reported in this paper.

Data availability

Data will be made available on request.

Acknowledgements

The research leading to these results has received funding from the Horizon 2020 Program, under Grant Agreement 952957, Trust-PV project.

The authors would also like to acknowledge the valuable contributions of the following companies.

Orange Climate Autarkis: A European based company involved in developing, producing, and bringing to market existing and innovative HVAC technologies and products, with the aim to create breakthrough innovations, impacting the sustainability transition.

Van Dorp Installaties is a Dutch-based HVAC installation company, involved in maintenance and upgrades of both existing and new buildings, with the specific aim of aiding its customers and stakeholders in the pathways towards reaching sustainability goals.

PV monitoring system. GHI, DHI, and DNI were measured using a Kipp & Zonen SOLYS2 [63] using SMP21 pyranometers and a SHP1 pyrliometer. Thermocouples were RS PRO type T. The value of power is obtained from the multiplication of the maximum power point current and voltage. The uncertainty is estimated using equation (A1).

Variable	Unit	Resolution	Uncertainty
Plane of array irradiance (G_{POA})	W/m^2	$7.63 \mu V/W/m^2$	$\pm 10 \mu V$
DHI, GHI, DNI	W/m^2	$7-14 \mu V/W/m^2$	$\pm 7 W/m^2$
V_{oc} , I_{sc}	V, A	3.8 mV, 15.2 μA	$\pm 0.1 mV, \pm 0.2 \mu A$
PV module temperature (T_{PV})	$^{\circ}C$	0.01 $^{\circ}C$	$\pm 0.5 ^{\circ}C$ or 0.4 %
Wind speed (Ws)	m/s	0.1 m/s	$\pm 0.5 m/s$
Ambient temperature (T_{amb})	$^{\circ}C$	0.01 $^{\circ}C$	$\pm 0.4 ^{\circ}C$
MPPT Voltage	V	20 mV (0–81.9V)	$\pm 0.1 mV, \pm 0.2 \mu A$
MPPT Current	A	2.5 mA (0–10.2A)	
Max. Module Power	W	Up to 300 W	$\pm 0.6 mW @ STC$

Table A 2 Number of data points used for analysis after filtering outliers. Each data point has a time resolution of 5 min. In total the data represents 4341 h of measurements.

Year	No. Data points
2019	3908
2020	11719
2021	36465

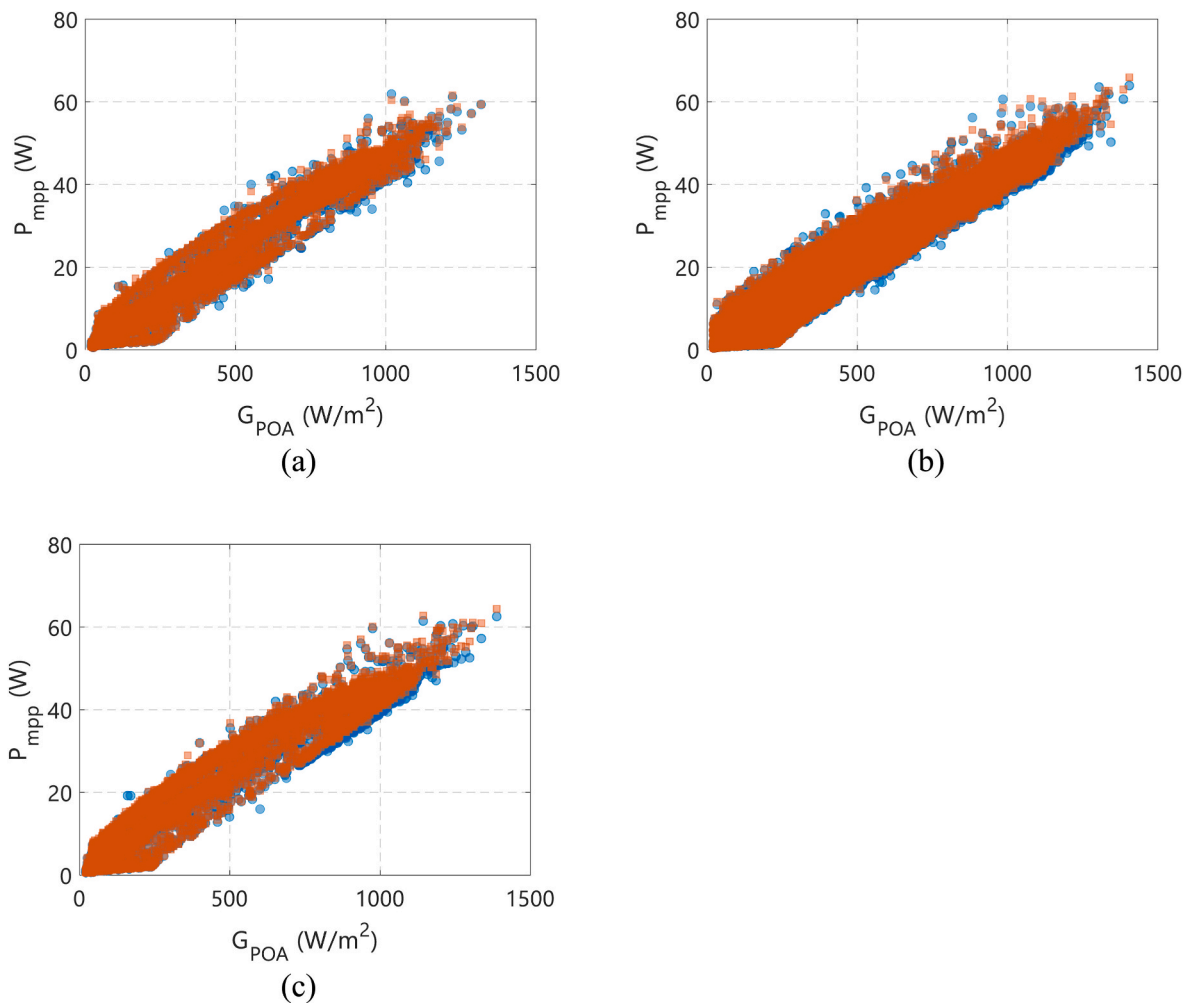


Figure A 1 Measured instantaneous DC power related to the measured G_{POA} for the standard module (blue points) and the PV-PCM module (orange squares) in Delft for the period (a) 2019, (b) 2020 and (c) 2021. All graphs present the final data after the elimination of outliers and desynchronized data that could potentially produce biases in the analysis. Additionally, the data presented here was compared to the resulting current, voltage, and power from a two-diode model to ensure good quality (see appendix).

B. Experimental work carried out at Catania, Italy

The experimental activities in Delft were finalized in August 2021, and the PV modules were uninstalled from the monitoring station and were characterized under the same LASS equipment used the previous time. EL imaging allowed the inspection of potential damage from the long-term activities. The results of these new measurements showed almost identical electrical parameters compared to the initial measurement. Furthermore, the obtained EL images showed that no damage was incurred during the testing period. Details of these tests are presented in the appendix.

The modules were shipped to ENEL facilities, located in Catania, Italy, at the end of September 2022. Figure B 1 presents photographs of the final setup.

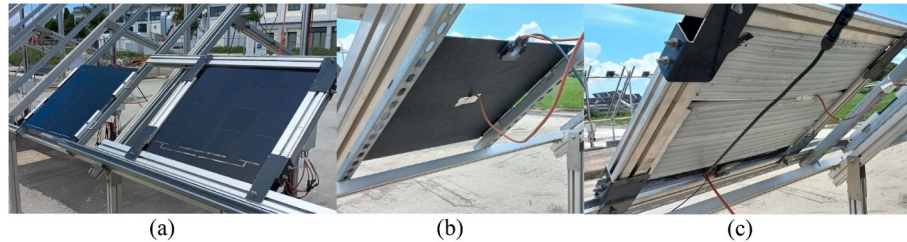


Fig. B1. Photographs of the installed PV modules at the facilities of ENEL, in Catania, Italy: (a) side by side view, (b) PV module rear view, and (c) PV-PCM module rear view. The backside of the modules in this location was not insulated during the tests. In (a) the PV-PCM module is on the right-hand side.

The measured variables at the facilities are summarized on Table B 1. The activities were carried out continuously from January until May 2023.

Table B 1 Measured variables at Enel Facilities in Catania, Italy. The value of power is obtained from the multiplication of the maximum power point current and voltage. The uncertainty is estimated using equation (A1)

Variable	Unit	Resolution	Uncertainty
Plane of array irradiance (G_{POA})	W/m^2	$8.5 \mu V/W/m^2$	$\pm 10 \mu V$
MPPT Voltage	V	1.0 mV	± 0.025 mV
MPPT Current	A	1.0 mA	± 0.1 mA
MPPT Power	W	–	± 0.15 mW @ STC
PV module temperature (T_{PV})	$^{\circ}C$	0.01 $^{\circ}C$	± 0.4 $^{\circ}C$
Wind speed (W_s)	m/s	0.01 m/s	0.4 m/s
Ambient temperature (T_{amb})	$^{\circ}C$	0.01 $^{\circ}C$	± 0.4 $^{\circ}C$

As in the case of the experiment in Delft, the data collected at ENEL facilities was filtered using both a linear relationship between the value of G_{POA} and the maximum power point current (I_{mpp}), and a two-diode model to compare the power measurements. The resulting data utilized for analysis is shown in Figure B 2(a) for the case of the maximum power point current, and Figure B 2(b) for the maximum power point voltage for both modules. In total, in Catania, 13550 data points were used for analysis, which represents nearly 1220 h of operation from January to May 2023.

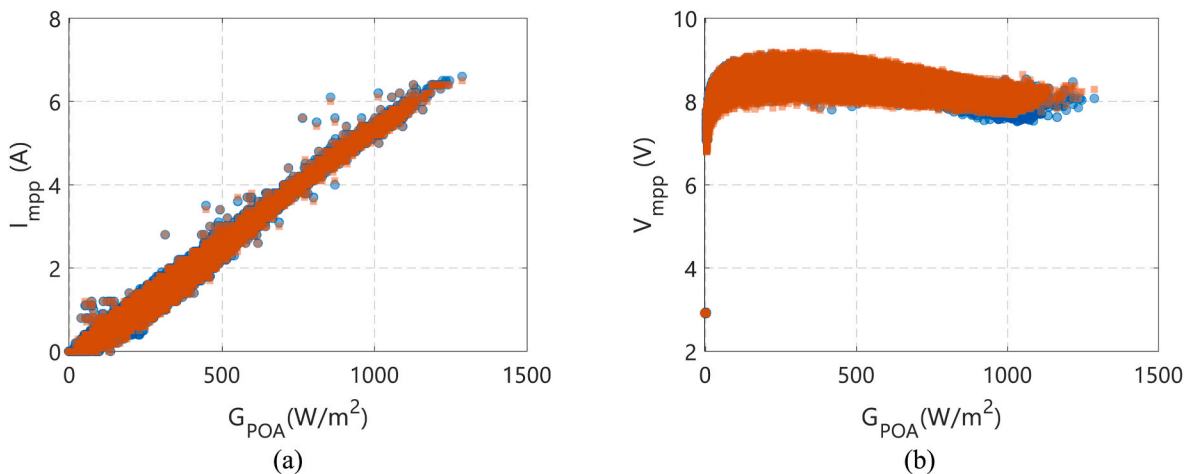


Fig. B2. Measured (blue points) and filtered (orange points) data with respect to the measured G_{POA} for the tests carried out in Catania, Italy: (a) maximum power point current (I_{mpp}) and maximum power point voltage (V_{mpp}).

C. Filtering and validation of electrical performance data

The filtering of the data for both locations consisted of comparing the measured electrical parameters from both PV modules with calculated values based on the measurements of plane of array irradiance (G_{POA}) and PV module temperature (T_{PV}). First, the measured short circuit current was compared to a calculated one, denoted as I_{SC-c} and estimated using following equation:

$$I_{SC-c} = \frac{G_{POA}}{G_{STC}} \cdot I_{SC-STC} - \rho_{ISC} \cdot (T_{STC} - T_{PV}) \tag{Eq A1}$$

Where G_{STC} and T_{STC} are the impinging irradiance and PV module temperature under standard tests conditions, respectively. ρ_{ISC} is the PV module's short circuit current temperature coefficient, which was assumed to be the same as that of the SunPower Maxeon Gen II solar cell (2.6 mA/°C).

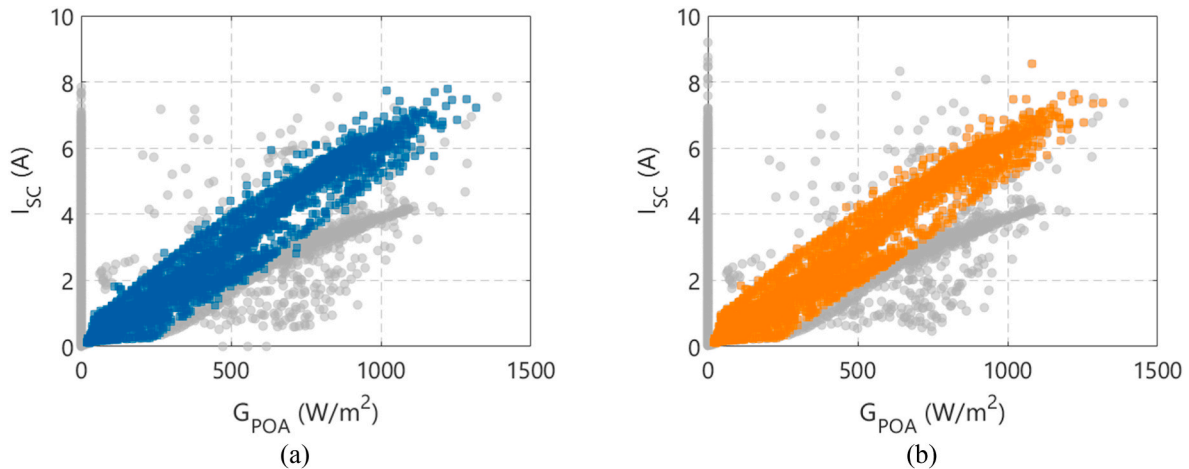


Fig. C1. (a) Unfiltered (grey circles) and filtered (colored squares) data based on Equation (A1) for the case of the standard PV module for year 2019 in Delft. (b) Unfiltered and filtered data based on Equation (A1) for the case of the PV-PCM for the year 2019 in Delft.

To filter potential erroneous data, the calculation of the difference between the value of I_{SC-c} with the measured one of I_{SC} was compared to a limiting value of $\pm 20\%$ of I_{SC-STC} , following the recommendations provided in the literature [64]. Any value greater or lower than this selected limit was considered unfit for analysis.

The second stage was to use a two-diode equivalent electrical circuit model to verify that the measured data was consistent with physical models and avoid potential biases produced by out-of-synch measurements, accidental shading of pyranometers and modules and other circumstances that might lead to measurement error. The required parameters for the equivalent circuit were extracted by using the tool from PV Lighthouse [65]. These values are presented in Table C 1. The initial fitting considered one single encapsulated cell, which was extracted from the measurement of the PV module and dividing its voltages by the number of cells in series (16). The final fitting shows good agreement with the measurement under STC conditions, as shown in Figure C 2. Once validated, this physical model was used to estimate the power that the module produces under different climatic conditions. Notice that, since the initial fitting considered the cell already encapsulated, the optical losses produced by the front glass and the encapsulant were already accounted for. The values used as input on the two-diode model were the measured G_{POA} and the measured operational temperature (T_{PV}) for Catania and the average measured operational temperature ($\overline{T_{PV}}$), for the validation of the data measured in Delft.

Table C 1 Two-diode parameters used for simulations.

Parameter		Unit	Value
Light collected current	(J_L)	(mA/cm ²)	36.87
Saturation current 1	(J_1)	(pA/cm ²)	0.38
Ideality factor 1	(m_1)	(-)	1.00
Saturation current 2	(J_2)	(nA/cm ²)	1.00
Ideality factor 2	(m_2)	(-)	2.00
Shunt resistance	(R_{SH})	(kΩ cm ²)	10.00
Series Resistance	(R_S)	(Ω cm ²)	1.50

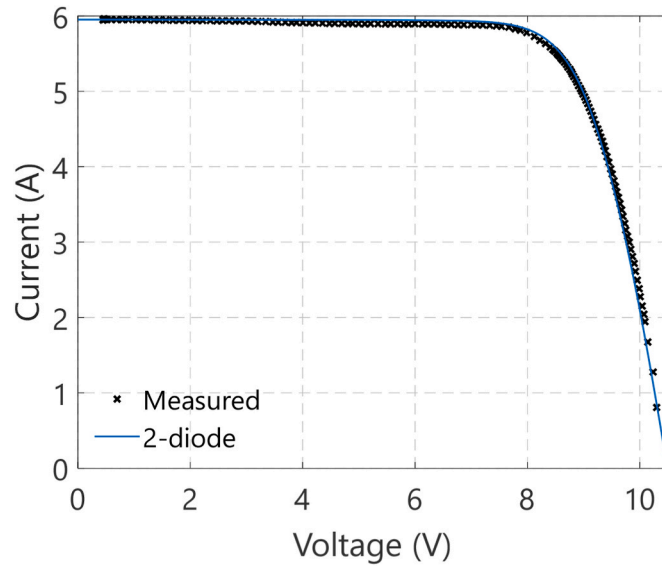


Fig. C2. Measured IV curve (denoted by X symbols), under STC conditions provided by the AAA class large area steady state (LASS) solar simulator. The module shown here would be then used to attach the PCM slabs on its backside (these laboratory measurements did not use any PCM). The two-diode equivalent circuit model use the parameters presented in Table A 1. The results show good agreement between the model and the measured module.

Figure C 3 showcases the results from this procedure. For the case of the standard module, some measured values of power deviate considerably from those estimated via the two-diode model. This same difference is not observed for the PV-PCM module, whose measured power values match those estimated with the two-diode model. Problems with the maximum power point tracking (MPPT) can be the reason for the discrepancy observed in the standard PV module.

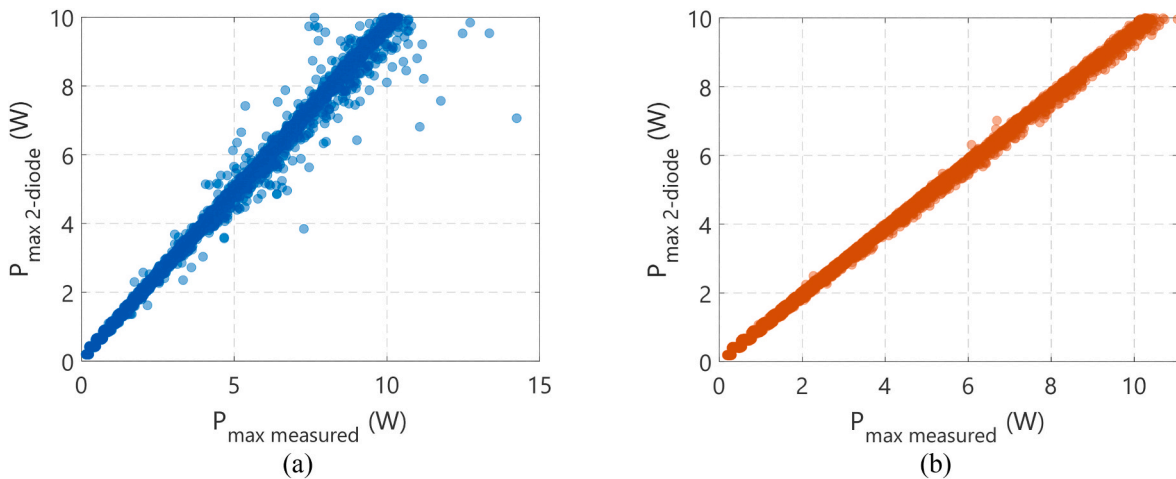


Fig. C3. (a) Measured and simulated value of the instantaneous maximum power of the standard PV module for the different environmental conditions (G_{POA} and $\overline{T_{PV}}$) in Delft from July 2019 to February 2020. (b) Measured and simulated value of the instantaneous maximum power of the PV-PCM module for the different environmental conditions (G_{POA} and $\overline{T_{PV}}$) in Delft from July 2019 to February 2020. Contrary to (a), in this case the fit of the model shows very good agreement. The errors observed on the standard module are more likely due to errors in the maximum power point tracking algorithm.

A final filter calculated the difference between the estimated value of P_{max} from the two-diode model and the one measured from the MPPT tracking software. Any value greater than 2 W or lower than -2 W was eliminated from both data sets (Standard module and PCM module). Overall, the errors obtained when comparing the modeled electrical parameters with the measured ones, for the period July 2019 to February 2020 in delft are as follows.

Table C 2 Errors for the modeled instantaneous power, via a two-diode model, compared to the measured values in Delft between July 2019 and February 2020.

Standard module		PCM module	
Error	Value	Parameter	Value
MAE _{pmax}	0.442 W	MAE _{pmax}	0.401 W
MBE _{pmax}	0.276 W	MBE _{pmax}	0.355 W
RMSE _{pmax}	1.113 W	RMSE _{pmax}	0.880 W

The data from Catania, Italy, was subjected to this same approach.

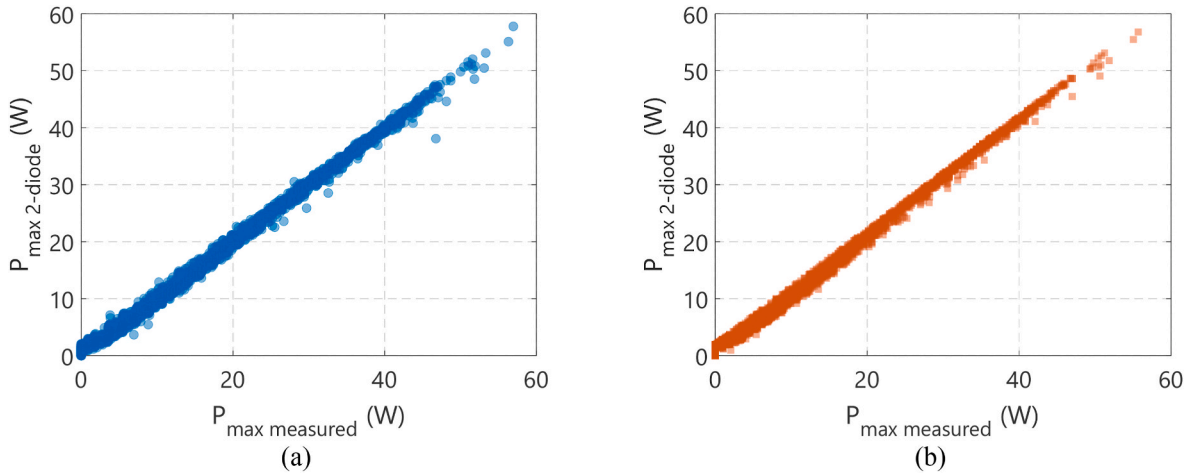


Fig. C4. (a) Measured and simulated value of the instantaneous maximum power of the standard PV module for the different environmental conditions (G_{POA} and T_{PV}) in Catania from January to May 2023. (b) Measured and simulated value of the instantaneous maximum power of the PV-PCM module for the different environmental conditions in Catania from January to May 2023.

Table C 3

Errors for the modeled instantaneous power, via a two-diode model, compared to the measured values in Catania between January and May 2023.

Standard module		PCM module	
Error	Value	Parameter	Value
MAE _{pmax}	0.204 W	MAE _{pmax}	0.290 W
MBE _{pmax}	-0.046 W	MBE _{pmax}	-0.250 W
RMSE _{pmax}	0.446 W	RMSE _{pmax}	0.598 W

D. Characterization of modules after the experiments done in Delft

The following are the results from the characterization tests done on the modules after the conclusion of the experiments conducted in Delft and before the measurements began in Catania.

Table D 1 Electrical parameters of the modules after the testing concluded in Delft.

Parameter	Standard	PCM
V_{OC} (V)	10.52	10.53
I_{SC} (A)	5.95	5.93
P_{mpp} (W)	46.98	46.77
η (%)	18.21	18.12

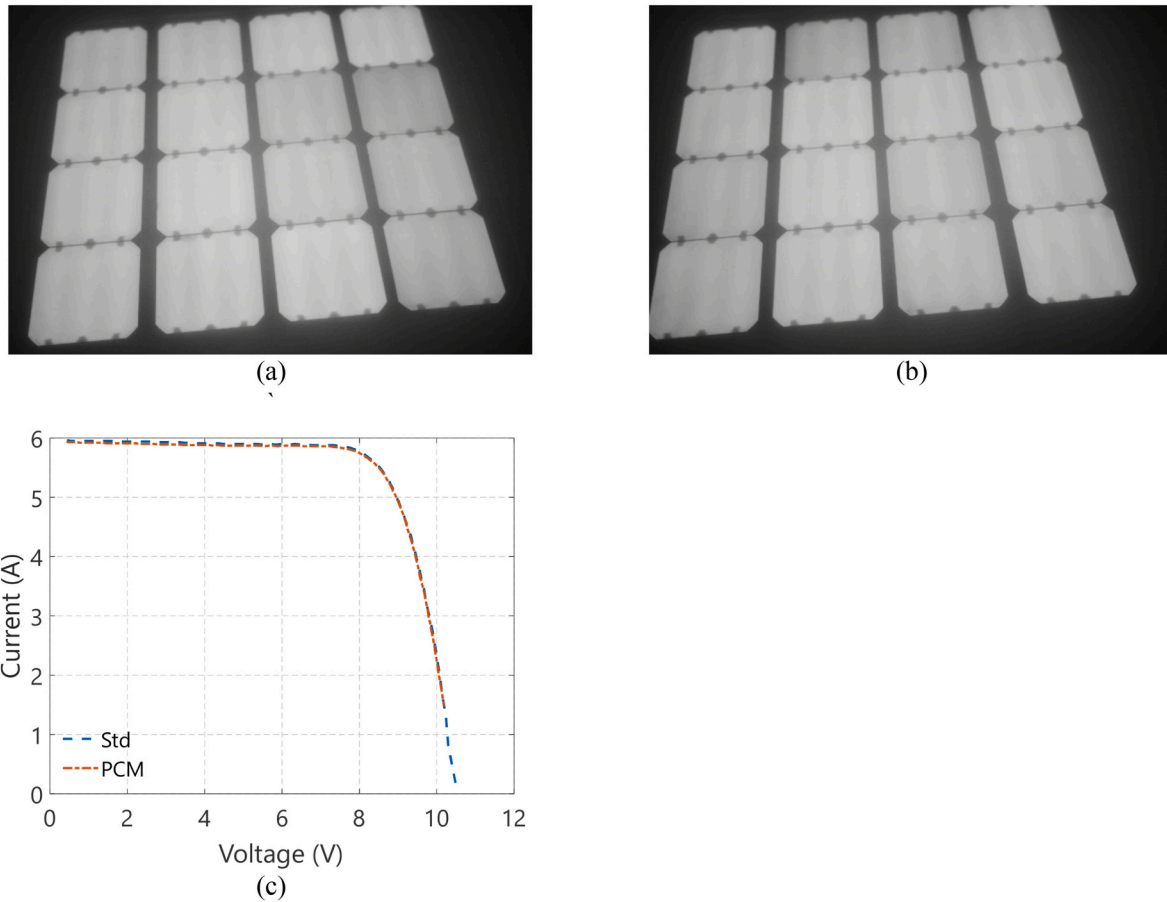


Fig. D1. (a) Electroluminescence image of the standard PV module after 3 years of operation without any maintenance. The images show no cracks or any other abnormalities on the module. (b) Similar to (a) for the case of the PV-PCM module, the integrity of the PV module was not hindered by the PCM slabs. (c) IV curve of both modules indicates no significant difference in performance between the modules. The second measurement shows a 1.69 % decrease in efficiency after three years of operation. However, the recorded irradiance value of each measurement differs by 2 %, with 1005 W/m^2 on the first compared to 988 W/m^2 , which can explain this difference.

E. Additional information of cooling potential for Delft (winter 2019–2020) and Catania (Spring 2023)

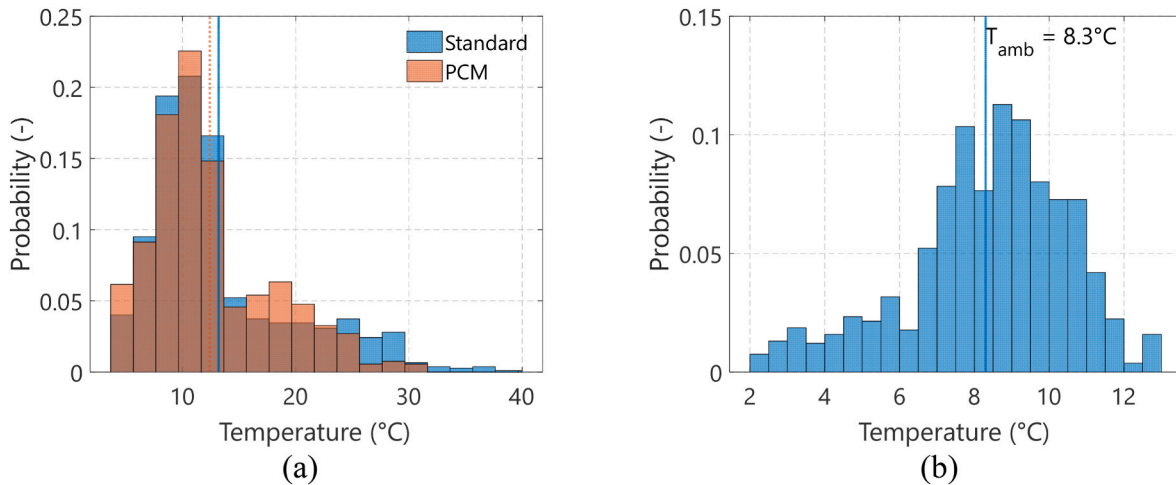


Fig. E1. (a) Histogram of the operational temperatures of the standard (Std) PV module and the PV-PCM module (PCM) for the winter days of 2019. (December 21, 2019, until February 8, 2020) between 9:00 and 15:00. The vertical lines indicate the mean values of the operating temperature of each module. Even during winter, the PV-PCM module presents lower operational temperatures. (b) Histogram of the measured ambient temperature for the same period described in (a).

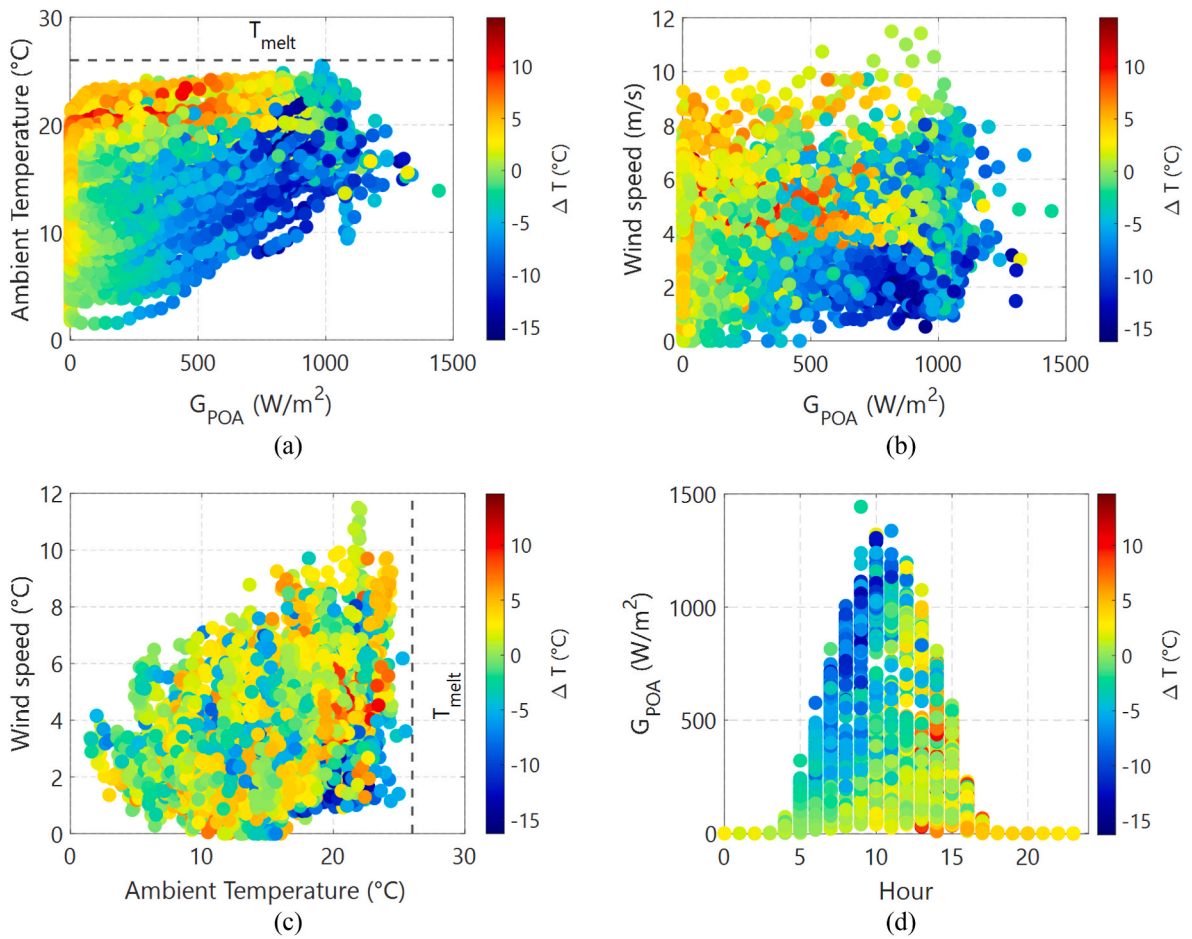


Fig. E2. (a) Influence of environmental conditions on the average temperature difference ΔT ($^{\circ}\text{C}$) during spring 2023 in Catania, Italy: (a) Effect of the ambient temperature related to the plane of array irradiance. The value of the melting temperature of the PCM is denoted by the dashed line; (b) effect of the windspeed related to the plane of array irradiance. (c) effect of the windspeed related to the ambient temperature; and (d) effect of the plane of array irradiance on the hourly temperature difference for the entire season.

F. Delft: Interannual variation in climatic conditions. Catania: Average climatic conditions

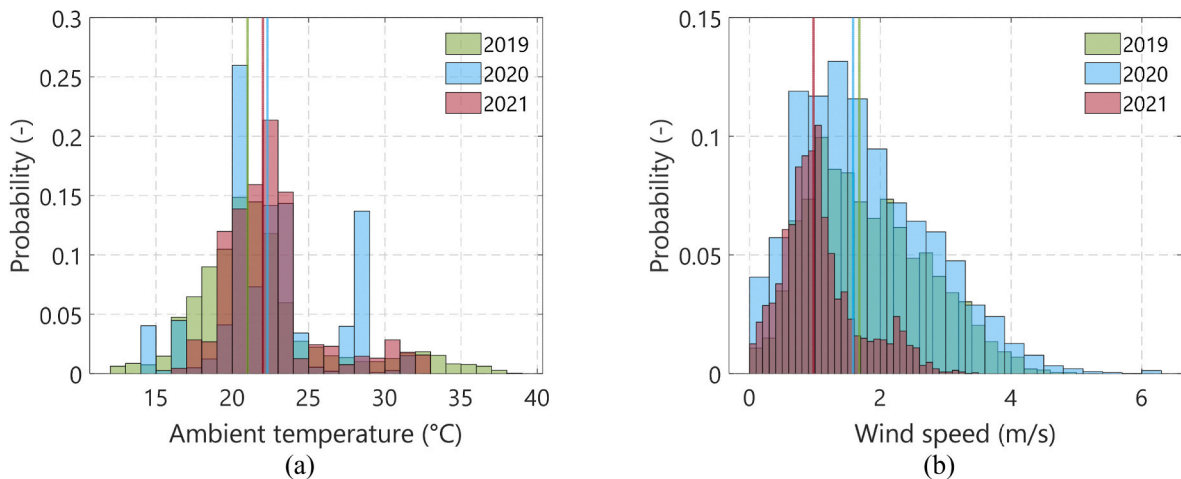


Fig. F1. (a) Histogram of ambient temperatures measured during the **summer** of 2019, 2020 and 2021 in Delft. The mean values of the recorded ambient temperatures for all years remain close (21°C in 2019, 22.3°C in 2020 and 22.0°C in 2021), which is consistent with the stable performance differences between both PV modules during these years. (b) Histogram of wind speed measured during the same season and years as (a). The data also reveals very high consistency between the years 2019 (1.67 m/s) and 2020 (1.58 m/s). During 2021, the mean measured windspeed was considerably lower (0.96 m/s). Nonetheless, the effect on overall energy yield was relatively small.

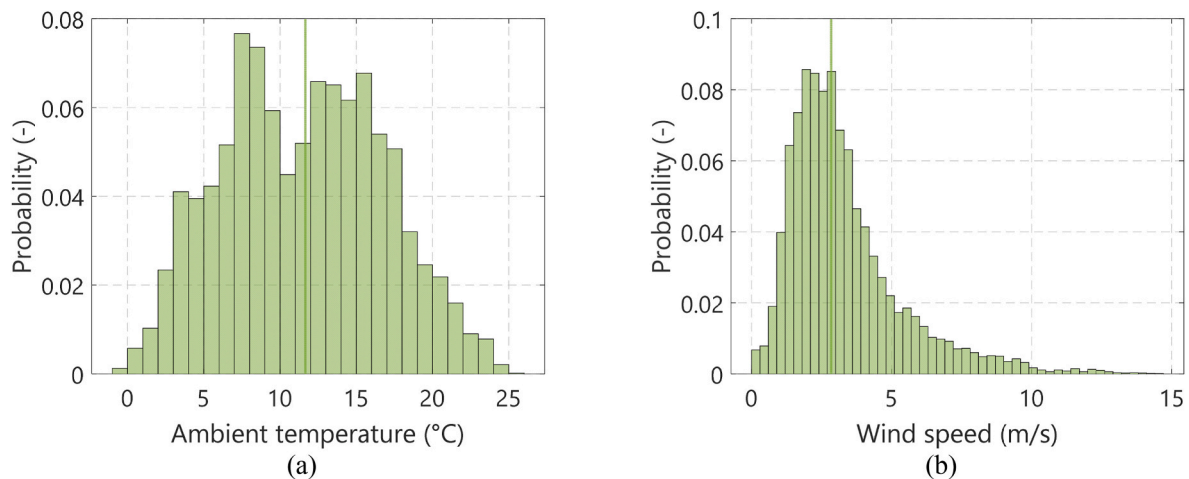


Fig. F2. (a) Histogram of ambient temperatures measured during the 2023 in Catania. The mean values of the recorded ambient temperatures were 12 °C. (b) Histogram of wind speed measured during the same season and years as (a) showcasing a mean value of 2.84 m/s. Even under these conditions, the PCM still provided benefit due to the high average irradiance reaching the panels.

References

- [1] I. Kaaya, J. Ascencio-Vásquez, K.A. Weiss, M. Topić, Assessment of uncertainties and variations in PV modules degradation rates and lifetime predictions using physical models, *Sol. Energy* 218 (June 2020) (2021) 354–367, <https://doi.org/10.1016/j.solener.2021.01.071>.
- [2] A. Gok, E. Ozkalay, G. Friesen, F. Frontini, The influence of operating temperature on the performance of BIPV modules; the influence of operating temperature on the performance of BIPV modules, *IEEE J Photovolt* 10 (5) (2020), <https://doi.org/10.1109/JPHOTOV.2020.3001181>.
- [3] R. Harahap, S. Suherman, Active versus passive cooling systems in increasing solar panel output, *Procedia Environmental Science, Engineering and Management* 8 (1) (2021) 157–166.
- [4] S. Nizetić, E. Giama, A.M. Papadopoulos, Comprehensive analysis and general economic-environmental evaluation of cooling techniques for photovoltaic panels, Part II: active cooling techniques, *Energy Convers. Manag.* 155 (Jan. 2018) 301–323, <https://doi.org/10.1016/j.enconman.2017.10.071>.
- [5] D. Sato, N. Yamada, Review of photovoltaic module cooling methods and performance evaluation of the radiative cooling method, *Renew. Energy* 104 (July 2018) (2019) 151–166, <https://doi.org/10.1016/j.renene.2018.12.051>.
- [6] N. Khorrami, M. Rajabi Zargarabadi, M. Dehghan, A novel spectrally selective radiation shield for cooling a photovoltaic module, *Sustain. Energy Technol. Assessments* 46 (April) (2021) 101269, <https://doi.org/10.1016/j.seta.2021.101269>.
- [7] P. Seokane da Silva, “Infrared Optical Filters for Passive Cooling of C-Si Solar Modules,” Delft University of Technology, Delft.
- [8] J.C. Ortiz Lizcano, et al., Practical design of an optical filter for thermal management of photovoltaic modules, *Prog. Photovoltaics Res. Appl.* (2024).
- [9] D. Vittorini, R. Cipollone, Fin-cooled photovoltaic module modeling – performances mapping and electric efficiency assessment under real operating conditions, *Energy* 167 (Jan. 2019) 159–167, <https://doi.org/10.1016/j.energy.2018.11.001>.
- [10] S. Khan, A. Waqas, N. Ahmad, M. Mahmood, N. Shahzad, M.B. Sajid, Thermal management of solar PV module by using hollow rectangular aluminum fins, *J. Renew. Sustain. Energy* 12 (6) (Nov. 2020), <https://doi.org/10.1063/5.0020129>.
- [11] F. Grubišić-Čabo, S. Nizetić, I. Marinić Kragić, D. Čoko, Further progress in the research of fin-based passive cooling technique for the free-standing silicon photovoltaic panels, *Int. J. Energy Res.* 43 (8) (Jun. 2019) 3475–3495, <https://doi.org/10.1002/er.4489>.
- [12] H.M. Maghrabie, A.S.A. Mohamed, A.M. Fahmy, A.A.A. Samee, Performance augmentation of PV panels using phase change material cooling technique: a review, *SVU-International Journal of Engineering Sciences and Applications* 2 (2) (2021) 1–13, <https://doi.org/10.21608/SVUJESA.2021.87202.1013>.
- [13] V.V. Tyagi, et al., A Comprehensive Review on Phase Change Materials for Heat Storage Applications: Development, Characterization, Thermal and Chemical Stability, Elsevier B.V., Jan. 01, 2022, <https://doi.org/10.1016/j.solmat.2021.111392>.
- [14] P. Zhang, X. Xiao, Z.W. Ma, A Review of the Composite Phase Change Materials: Fabrication, Characterization, Mathematical Modeling and Application to Performance Enhancement, Elsevier Ltd., Mar. 01, 2016, <https://doi.org/10.1016/j.apenergy.2015.12.043>.
- [15] I. Shamseddine, F. Penneç, P. Biwole, F. Fardoun, Supercooling of Phase Change Materials: A Review, Elsevier Ltd., Apr. 01, 2022, <https://doi.org/10.1016/j.rser.2022.112172>.
- [16] E. Japs, G. Sonnenrein, J. Steube, J. Vrabec, E. Kenig, S. Krauter, Technical Investigation of Photovoltaic module with integrated improved phase change material, in: *28th European Photovoltaic Solar Energy Conference And Exhibition, EUPVSEC*, 2013, pp. 500–502.
- [17] S. Maiti, S. Banerjee, K. Vyas, P. Patel, P.K. Ghosh, Self regulation of photovoltaic module temperature in V-trough using a metal-wax composite phase change matrix, *Sol. Energy* 85 (9) (Sep. 2011) 1805–1816, <https://doi.org/10.1016/j.solener.2011.04.021>.
- [18] S. Sharma, L. Micheli, W. Chang, A.A. Tahir, K.S. Reddy, T.K. Mallick, Nano-enhanced phase change material for thermal management of BICPV, *Appl. Energy* 208 (Dec. 2017) 719–733, <https://doi.org/10.1016/j.apenergy.2017.09.076>.
- [19] A. Hasan, J. Sarwar, H. Alnoman, S. Abdelbaqi, Yearly energy performance of a photovoltaic-phase change material (PV-PCM) system in hot climate, *Sol. Energy* 146 (2017) 417–429, <https://doi.org/10.1016/j.solener.2017.01.070>.
- [20] R. Stropnik, U. Strith, Increasing the efficiency of PV panel with the use of PCM, *Renew. Energy* 97 (Nov. 2016) 671–679, <https://doi.org/10.1016/j.renene.2016.06.011>.
- [21] R. Madurai Elavarasan, M. Nadarajah, R. Pugazhendhi, S. Gangatharan, An experimental investigation on coalescing the potentiality of PCM, fins and water to achieve sturdy cooling effect on PV panels, *Appl. Energy* 356 (Feb) (2024), <https://doi.org/10.1016/j.apenergy.2023.122371>.
- [22] K.S. Kumar, S. Revanth, D. Sanjeev, P.S. Kumar, P. Surya, Experimental investigation of improving the energy conversion efficiency of PV cell by integrating with PCM, in: *Materials Today: Proceedings*, Elsevier Ltd, 2020, pp. 712–716, <https://doi.org/10.1016/j.matpr.2020.05.723>.
- [23] A. Karthick, K. Kalidasa Murugavel, A. Ghosh, K. Sudhakar, P. Ramanan, Investigation of a binary eutectic mixture of phase change material for building integrated photovoltaic (BIPV) system, *Sol. Energy Mater. Sol. Cell.* 207 (Apr. 2020), <https://doi.org/10.1016/j.solmat.2019.110360>.
- [24] P. Singh, V. Mudgal, S. Khanna, T.K. Mallick, K.S. Reddy, Experimental investigation of solar photovoltaic panel integrated with phase change material and multiple conductivity-enhancing-containers, *Energy* 205 (Aug) (2020), <https://doi.org/10.1016/j.energy.2020.118047>.
- [25] A. Waqas, J. Ji, A. Bahadar, L. Xu, Zeshan, M. Modjinou, Thermal management of conventional photovoltaic module using phase change materials—an experimental investigation, *Energy Explor. Exploit.* 37 (5) (Sep. 2019) 1516–1540, <https://doi.org/10.1177/0144598718795697>.
- [26] T. Wongwuttanasatien, T. Sarikarin, A. Sukrsi, Performance enhancement of a photovoltaic module by passive cooling using phase change material in a finned container heat sink, *Sol. Energy* 195 (Jan. 2020) 47–53, <https://doi.org/10.1016/j.solener.2019.11.053>.
- [27] N. Choubineh, H. Jannesari, A. Kasaean, Experimental study of the effect of using phase change materials on the performance of an air-cooled photovoltaic system, *Renew. Sustain. Energy Rev.* 101 (Mar. 2019) 103–111, <https://doi.org/10.1016/j.rser.2018.11.001>.
- [28] F. Rajae, M.A.V. Rad, A. Kasaean, O. Mahian, W.M. Yan, Experimental analysis of a photovoltaic/thermoelectric generator using cobalt oxide nanofluid and phase change material heat sink, *Energy Convers. Manag.* 212 (May 2020), <https://doi.org/10.1016/j.enconman.2020.112780>.
- [29] E. Klugmann-Radziemska, P. Wcislo-Kucharek, Photovoltaic module temperature stabilization with the use of phase change materials, *Sol. Energy* 150 (Jul. 2017) 538–545, <https://doi.org/10.1016/j.solener.2017.05.016>.

- [30] H.M. Ali, Recent Advancements in PV Cooling and Efficiency Enhancement Integrating Phase Change Materials Based Systems – A Comprehensive Review, Elsevier Ltd., Feb. 01, 2020, <https://doi.org/10.1016/j.solener.2019.11.075>.
- [31] P.H. Biwole, P. Eclache, F. Kuznik, Phase-change materials to improve solar panel's performance, *Energy Build.* 62 (2013) 59–67, <https://doi.org/10.1016/j.enbuild.2013.02.059>.
- [32] Y. Dutil, D.R. Rousse, N. Ben Salah, S. Lassue, L. Zalewski, A Review on Phase-Change Materials: Mathematical Modeling and Simulations, *Jan.* 2011, <https://doi.org/10.1016/j.rser.2010.06.011>.
- [33] M.J. Huang, P.C. Eames, B. Norton, Phase change materials for limiting temperature rise in building integrated photovoltaics, *Sol. Energy* 80 (9) (Sep. 2006) 1121–1130, <https://doi.org/10.1016/j.solener.2005.10.006>.
- [34] K. Kant, A. Shukla, A. Sharma, P.H. Biwole, Heat transfer studies of photovoltaic panel coupled with phase change material, *Sol. Energy* 140 (Dec. 2016) 151–161, <https://doi.org/10.1016/j.solener.2016.11.006>.
- [35] S. Khanna, K.S. Reddy, T.K. Mallick, Optimization of finned solar photovoltaic phase change material (finned pv pcm) system, *Int. J. Therm. Sci.* 130 (Aug. 2018) 313–322, <https://doi.org/10.1016/j.ijthermalsci.2018.04.033>.
- [36] M. Tao, L. Zhenpeng, Z. Jiaxin, Photovoltaic Panel Integrated with Phase Change Materials (PV-PCM): Technology Overview and Materials Selection, Elsevier Ltd., Dec. 01, 2019, <https://doi.org/10.1016/j.rser.2019.109406>.
- [37] S. Preet, A Review on the Outlook of Thermal Management of Photovoltaic Panel Using Phase Change Material, Elsevier Ltd., Dec. 01, 2021, <https://doi.org/10.1016/j.egycc.2021.100033>.
- [38] SOLARGIS, "SOLARGIS Prospect," <https://apps.solargis.com/prospect/map?c=47.680183,18.039551,5&s=52.187405,4.570313&m=solargis-d2g&l=true>.
- [39] Orange Climate Autarkis, "Orange Climate Autarkis: Phase Transition Materials," <https://www.orangeclimate.com/nl/oc-producten>.
- [40] P. van den Engel, M. Malin, N.K. Venkatesh, L.A. de Araujo Passos, Performance of a phase change material battery in a transparent building, *Fluid Dynam. Mater. Process.* 19 (3) (2023) 783–805, <https://doi.org/10.32604/fdmp.2022.021962>.
- [41] S.P. Corporation, MAXEON™ GEN III SOLAR CELLS Electrical Characteristics of a Typical Maxeon Gen III Cell, 2017, pp. 3–4.
- [42] B. Kamkari, H. Shokouhmand, Experimental investigation of phase change material melting in rectangular enclosures with horizontal partial fins, *Int. J. Heat Mass Tran.* 78 (2014) 839–851, <https://doi.org/10.1016/j.ijheatmasstransfer.2014.07.056>.
- [43] M. Fadl, P. Eames, A numerical investigation into the heat transfer and melting process of lauric acid in a rectangular enclosure with three values of wall heat flux, in: *Energy Procedia*, Elsevier Ltd, 2019, pp. 4502–4509, <https://doi.org/10.1016/j.egypro.2019.01.761>.
- [44] N. Mallya, S. Haussener, Buoyancy-driven melting and solidification heat transfer analysis in encapsulated phase change materials, *Int. J. Heat Mass Tran.* 164 (Jan) (2021), <https://doi.org/10.1016/j.ijheatmasstransfer.2020.120525>.
- [45] K. Kant, A. Shukla, A. Sharma, P.H. Biwole, Heat transfer studies of photovoltaic panel coupled with phase change material, *Sol. Energy* 140 (Dec. 2016) 151–161, <https://doi.org/10.1016/j.solener.2016.11.006>.
- [46] K. Kant, A. Shukla, A. Sharma, P.H. Biwole, Melting and solidification behaviour of phase change materials with cyclic heating and cooling, *J. Energy Storage* 15 (Feb. 2018) 274–282, <https://doi.org/10.1016/j.est.2017.12.005>.
- [47] A. Shukla, K. Kant, P.H. Biwole, R. Pitchumani, A. Sharma, Melting and solidification of a phase change material with constructal tree-shaped fins for thermal energy storage, *J. Energy Storage* 53 (Sep) (2022), <https://doi.org/10.1016/j.est.2022.105158>.
- [48] J. Sutradhar, R. Kothari, S.K. Sahu, Solidification and melting model of phase change material with volumetric shrinkage/expansion void in an annulus, *Appl. Therm. Eng.* 195 (Aug) (2021), <https://doi.org/10.1016/j.applthermaleng.2021.117202>.
- [49] T. Sathe, A.S. Dhoble, Thermal analysis of an inclined heat sink with finned PCM container for solar applications, *Int. J. Heat Mass Tran.* 144 (Dec) (2019), <https://doi.org/10.1016/j.ijheatmasstransfer.2019.118679>.
- [50] Y. Hong, W.B. Ye, S.M. Huang, M. Yang, J. Du, Thermal storage characteristics for rectangular cavity with partially active walls, *Int. J. Heat Mass Tran.* 126 (Nov. 2018) 683–702, <https://doi.org/10.1016/j.ijheatmasstransfer.2018.05.005>.
- [51] P.H. Biwole, D. Groulx, F. Souayfane, T. Chiu, Influence of fin size and distribution on solid-liquid phase change in a rectangular enclosure, *Int. J. Therm. Sci.* 124 (Feb. 2018) 433–446, <https://doi.org/10.1016/j.ijthermalsci.2017.10.038>.
- [52] V. Joshi, M.K. Rathod, Constructal enhancement of thermal transport in latent heat storage systems assisted with fins, *Int. J. Therm. Sci.* 145 (Nov) (2019), <https://doi.org/10.1016/j.ijthermalsci.2019.105984>.
- [53] M. Arıcı, E. Tütüncü, Ç. Yıldız, D. Li, Enhancement of PCM melting rate via internal fin and nanoparticles, *Int. J. Heat Mass Tran.* 156 (Aug) (2020), <https://doi.org/10.1016/j.ijheatmasstransfer.2020.119845>.
- [54] S.L. Tariq, H.M. Ali, M.A. Akram, M.M. Janjua, M. Ahmadlouydarab, Nanoparticles Enhanced Phase Change Materials (NePCMs)-A Recent Review, Elsevier Ltd., Jul. 25, 2020, <https://doi.org/10.1016/j.applthermaleng.2020.115305>.
- [55] J. Sarwar, S. McCormack, M.J. Huang, B. Norton, Experimental validation of CFD modelling for thermal regulation of Photovoltaic panels using phase change material, in: *International Conference for Sustainable Energy Storage*, Feb. 2011. Belfast.
- [56] M.P.F. Verheijen, *Thermal Management of Photovoltaics Using Phase Change Materials*, Delft University of Technology, Delft, 2019.
- [57] Gütegemeinschaft PCM e.V., "Quality Association PCM," <https://www.pcm-ral.org/pcm/en/quality-association-pcm/>.
- [58] I. Kaaya, A. Alzade, A. Tuomiranta, J. Ascencio-Vásquez, D. Saelens, I. Gordon, Lifetime prediction of photovoltaic modules: towards a generalized physics-based approach, in: *8th World Conference on Photovoltaic Energy Conversion*, Milan, 2022.
- [59] I. Kaaya, S. Lindig, K.A. Weiss, A. Virtuani, M. Sidrach de Cardona Ortin, D. Moser, Photovoltaic lifetime forecast model based on degradation patterns, *Prog. Photovoltaics Res. Appl.* 28 (10) (2020) 979–992, <https://doi.org/10.1002/pip.3280>.
- [60] I. Kaaya, M. Koehl, A.P. Mehilli, S. De Cardona Mariano, K.A. Weiss, Modeling outdoor service lifetime prediction of PV modules: effects of combined climatic stressors on PV module power degradation, *IEEE J Photovolt* 9 (4) (2019) 1105–1112, <https://doi.org/10.1109/JPHOTOV.2019.2916197>.
- [61] C.J. Smith, P.M. Forster, R. Crook, Global analysis of photovoltaic energy output enhanced by phase change material cooling, *Appl. Energy* 126 (Aug. 2014) 21–28, <https://doi.org/10.1016/j.apenergy.2014.03.083>.
- [62] U. of L. Lpvo, *PV Monitoring Solutions*, 2023. Ljubljana.
- [63] Kipp and Zonen, "SOLYS2 Sun Tracker," <https://www.kippzonen.com/Product/20/SOLYS2-Sun-Tracker>.
- [64] A. Livera et al., "Guidelines for ensuring data quality for photovoltaic system performance assessment and monitoring PV-ESTIA-Enhancing storage integration in buildings with Photovoltaics View project 37th European Photovoltaic Solar Energy Conference and Exhibition GUIDELINES FOR ENSURING DATA QUALITY FOR PHOTOVOLTAIC SYSTEM PERFORMANCE ASSESSMENT AND MONITORING." [Online]. Available: <https://www.researchgate.net/publication/344269813>.
- [65] P. Lighthouse, "PV Lighthouse: Equivalent-circuit calculator." Accessed: October. 21, 2022. [Online]. Available: <https://www.pvlighthouse.com.au>.